North-South asymmetry in the modeled phytoplankton community response to climate change over the 21st century

Irina Marinov,[1,2] Scott C. Doney,[2] Ivan D. Lima,[2] K. Lindsay,[3] J. K. Moore,[4] and N. Mahowald[5]

Received 28 February 2013; revised 23 October 2013; accepted 26 October 2013; published 20 December 2013.

[1] Here we analyze the impact of projected climate change on plankton ecology in all major ocean biomes over the 21st century, using a multidecade (1880–2090) experiment conducted with the Community Climate System Model (CCSM-3.1) coupled ocean-atmosphere-land-sea ice model. The climate response differs fundamentally in the Northern and Southern Hemispheres for diatom and small phytoplankton biomass and consequently for total biomass, primary, and export production. Increasing vertical stratification in the Northern Hemisphere oceans decreases the nutrient supply to the ocean surface. Resulting decreases in diatom and small phytoplankton biomass together with a relative shift from diatoms to small phytoplankton in the Northern Hemisphere result in decreases in the total primary and export production and export ratio, and a shift to a more oligotrophic, more efficiently recycled, lower biomass euphotic layer. By contrast, temperature and stratification increases are smaller in the Southern compared to the Northern Hemisphere. Additionally, a southward shift and increase in strength of the Southern Ocean westerlies act against increasing temperature and freshwater fluxes to destratify the water-column. The wind-driven, poleward shift in the Southern Ocean subpolar-subtropical boundary results in a poleward shift and increase in the frontal diatom bloom. This boundary shift, localized increases in iron supply, and the direct impact of warming temperatures on phytoplankton growth result in diatom increases in the Southern Hemisphere. An increase in diatoms and decrease in small phytoplankton partly compensate such that while total production and the efficiency of organic matter export to the deep ocean increase, total Southern Hemisphere biomass does not change substantially. The impact of ecological shifts on the global carbon cycle is complex and varies across ecological biomes, with Northern and Southern Hemisphere effects on the biological production and export partially compensating. The net result of climate change is a small Northern Hemisphere-driven decrease in total primary production and efficiency of organic matter export to the deep ocean.

Citation: Marinov, I., S. C. Doney, I. D. Lima, K. Lindsay, J. K. Moore, and N. Mahowald (2013), North-South asymmetry in the modeled phytoplankton community response to climate change over the 21st century, *Global Biogeochem. Cycles*, *27*, 1274–1290, doi:10.1002/2013GB004599.

1. Introduction

[2] Phytoplankton are a critical component of the oceanic biological pump, taking up nutrients and inorganic carbon from the ocean surface through photosynthesis and contributing to their downward transport to the subsurface ocean via the subsequent sinking and remineralization of organic and inorganic particulate matter. Diatoms are heavy silicified phytoplankton that sink fast and are generally thought to be better at exporting carbon to the subsurface ocean compared to the lighter picoplankton and nanoplankton, collectively referred to here as small phytoplankton. Climate-induced changes in the relative contribution of diatoms and small phytoplankton might, therefore, significantly affect export production (i.e., the export of particulate organic matter out of the euphotic layer) and the net carbon sequestration in the ocean [e.g., *Falkowski et al.*, 1998; *Cermeno et al.*, 2008]. Predicting future changes is complicated by the fact that climate change will impact simultaneously temperature, light availability, and nutrients, each of which affect the relative abundance of species differentially [*Marinov et al.*, 2010].

[3] Anthropogenic addition of CO_2 to the atmosphere is projected to result in warming of the upper ocean, accelerated melting of land ice, strengthening of the hydrological cycle and freshening of the high-latitude oceans, and retreat of sea

Additional supporting information may be found in the online version of this article.

[1]Department of Earth and Environmental Science, University of Pennsylvania, Philadelphia, Pennsylvania, USA.
[2]Department of Marine Chemistry and Geochemistry, Woods Hole Oceanographic Institution, Woods Hole, Massachusetts, USA.
[3]Climate and Global Dynamics Division, National Center for Atmosphere Research, Boulder, Colorado, USA.
[4]Department of Earth System Science, Univ. of California at Irvine, Irvine, California, USA.
[5]Department of Earth and Atmospheric Sciences, Cornell University, Ithaca, New York, USA.

Corresponding author: I. Marinov, Department of Earth and Environmental Science, University of Pennsylvania, 240 S. 33rd St., Hayden Hall, Philadelphia, PA 19104, USA. (imarinov@sas.upenn.edu)

0886-6236/13/10.1002/2013GB004599

ice [*Solomon et al*., 2007]. The combined effect is to stratify most of the upper ocean. Global models [e.g., *Bopp et al*., 2001; *Sarmiento et al*., 2004; *Bopp et al*., 2005; *Steinacher et al*., 2010] and first-order principles [*Doney*, 2006] have hence projected a decrease in surface nutrient supply to phytoplankton and ocean productivity in low-latitude and midlatitude and an increase in light exposure for phytoplankton and productivity in high latitudes. Detecting a climate change-driven trend in ocean ecology from observations, however, is far from trivial given natural interannual to decadal variability, the limited duration and sparse global observational records and the fact that the productivity changes can go in either direction. For example, a recent study predicts that we need ~40 more years of satellite color to distinguish an anthropogenic warming signal from the natural variability in the system [*Henson et al*., 2010; see also *Yoder et al*., 2010]. Analyses of satellite observations indicate both increases [*Gregg et al*., 2005; *Antoine et al*., 2005] and decreases [*Gregg et al*., 2003] in total chlorophyll over the past few decades. Others have observed regional temporal correlations between SSTs and chlorophyll from satellite color data [e.g., *Behrenfeld et al*., 2006; *Martinez et al*., 2009; *Siegel et al*., 2013] or spatial correlations between phytoplankton community composition and nutricline depth from ship transects [*Cermeno et al*., 2008] that could be used empirically to extrapolate to future climate change projections.

[4] Projected future climate change will result in a south-to-north warming asymmetry, with both atmospheric and ocean surface temperatures increasing much less in the Southern Hemisphere (SH) compared to the Northern Hemisphere (NH) [*Meehl et al*., 2007]. In climate modeling studies, this has been largely attributed to more ocean coverage and hence larger heat capacity and thermal inertia in the SH compared to the NH [e.g., *Bryan et al*., 1988; *Manabe et al*., 1991; *Flato and Boer*, 2001]. Higher evaporative latent heat loss over the oceans and a strong ice-albedo positive feedback in the Arctic further enhance the interhemispheric asymmetry [*Wang and Overland*, 2009]. *Hutchinson et al*. [2013] claim that part of the asymmetry is due to the thermal isolation of the Southern Ocean provided by the Antarctic Circumpolar Current. By contrast, sulfate aerosols are expected to cool the NH more than the SH [*Dufresne et al*., 2005], reducing this asymmetry. In the present paper, we show that this North-South asymmetry in warming will contribute to an asymmetry in oceanic biogeochemical and ecological responses to 21st century climate change.

[5] Southern Ocean westerlies drive deep-water upwelling, exposing nutrient and carbon-rich deep waters to the surface. Increases in these winds were shown to lead to increased outgassing of deep-ocean CO_2 and increased atmospheric CO_2 on long, equilibrium time scales [e.g., *Marinov et al*., 2008]. *Toggweiler et al*. [2006] proposed that wind changes might account for glacial-interglacial variations in atmospheric pCO_2. Researchers have also documented a poleward shift and strengthening of the midlatitude westerly winds in both hemispheres over the past few decades [*Thompson and Solomon*, 2002]. Recent modeling work has focused on the impact of increasing Southern Ocean westerlies on future anthropogenic carbon uptake [*Russell et al*., 2006] or on present day CO_2 outgassing from the Southern Ocean [*Lovenduski et al*., 2007; *Le Quere et al*., 2007; *Lovenduski et al*., 2008; (Bernardello et al., Response of ocean natural carbon storage under projected 21st century climate change, accepted, *Journal of Climate,* 2013)]. While our understanding of the temporal and spatial evolution of midlatitude westerlies and their impact on ocean biogeochemistry has been gradually improving, the net impact of these wind shifts on ocean phytoplankton ecology and the subsequent implications for ocean carbon storage are far less studied. Our work attempts to fill in this gap.

[6] In the present paper, we analyze the response of surface ocean phytoplankton ecology to 21st century climate change using a coupled global carbon cycle-climate model with an ecosystem component, following in the footsteps of recent studies which used similar tools [e.g., *Bopp et al*., 2001, 2005; *Schmittner et al*., 2008, 2010; *Gnanadesikan et al*., 2011; *Taucher and Oschlies*, 2011; *Bopp et al*., 2013]. Unlike these previous studies we focus here on (1) a systematic analysis of ecosystem responses across all ecological biomes, separating the nutrient, temperature, and light-driven phytoplankton responses and (2) the different and at times opposite ecological and biogeochemical responses in corresponding NH and SH biomes.

[7] Our previous work [*Marinov et al*., 2010], provides a theoretical framework for the present discussion. In particular, a linear Taylor analysis of the CCSM-3 model equations allows us to separate climate-driven changes in growth rate for each phytoplankton type into light, nutrient, and temperature components (equations (A5) and (A6a), (A6b), (A6c) in Appendix A). This separation is performed for each ecological biome to support our discussion in section 3.

2. Methods

[8] Our results are based on global numerical simulations using the midrange spatial resolution version of the Community Climate System Model version 3 (CCSM-3) [*Yeager et al*., 2006], to which prognostic land and ocean carbon cycle and ecosystem dynamics were added; the simulations analyzed here are the same as those described and reported in *Thornton et al*. [2009] and *Mahowald et al*. [2010]. The ocean physics component of CCSM-3 is the Parallel Ocean Program (POP), a z-level, hydrostatic, primitive equation model [*Smith and Gent*, 2002; *Collins et al*., 2006]. The version integrated here has the gx3v5 resolution, i.e., 3.6° in longitude, 0.8° to 1.8° in latitude (finer resolution near the equator), and 25 vertical levels with level thickness monotonically increasing from approximately 12 to 450 m [*Yeager et al*., 2006]. The biogeochemistry-ecosystem-circulation (BEC) ocean component consists of upper ocean ecological [*Moore et al*., 2002, 2004] and full depth biogeochemical [*Doney et al*., 2006] modules embedded in POP. This model includes a carbonate chemistry module, which dynamically calculates surface pCO_2 from simulated temperature, salinity, dissolved inorganic carbon, and total alkalinity, as well as air-sea gas exchange for CO_2 and O_2 [*Doney et al*., 2006]. A dynamical iron cycle is incorporated with seasonally varying atmospheric dust deposition, water-column scavenging, and continental sediment source.

[9] BEC includes three phytoplankton groups: a small phytoplankton class (which incorporates nanoplakton/picoplankton and coccolithophores), nitrogen-fixing diazotrophs, and diatoms, with growth parameterizations detailed in Appendix A (equations (A1), (A2), (A3), (A4)). A single zooplankton class grazes differentially on the phytoplankton groups. Additional

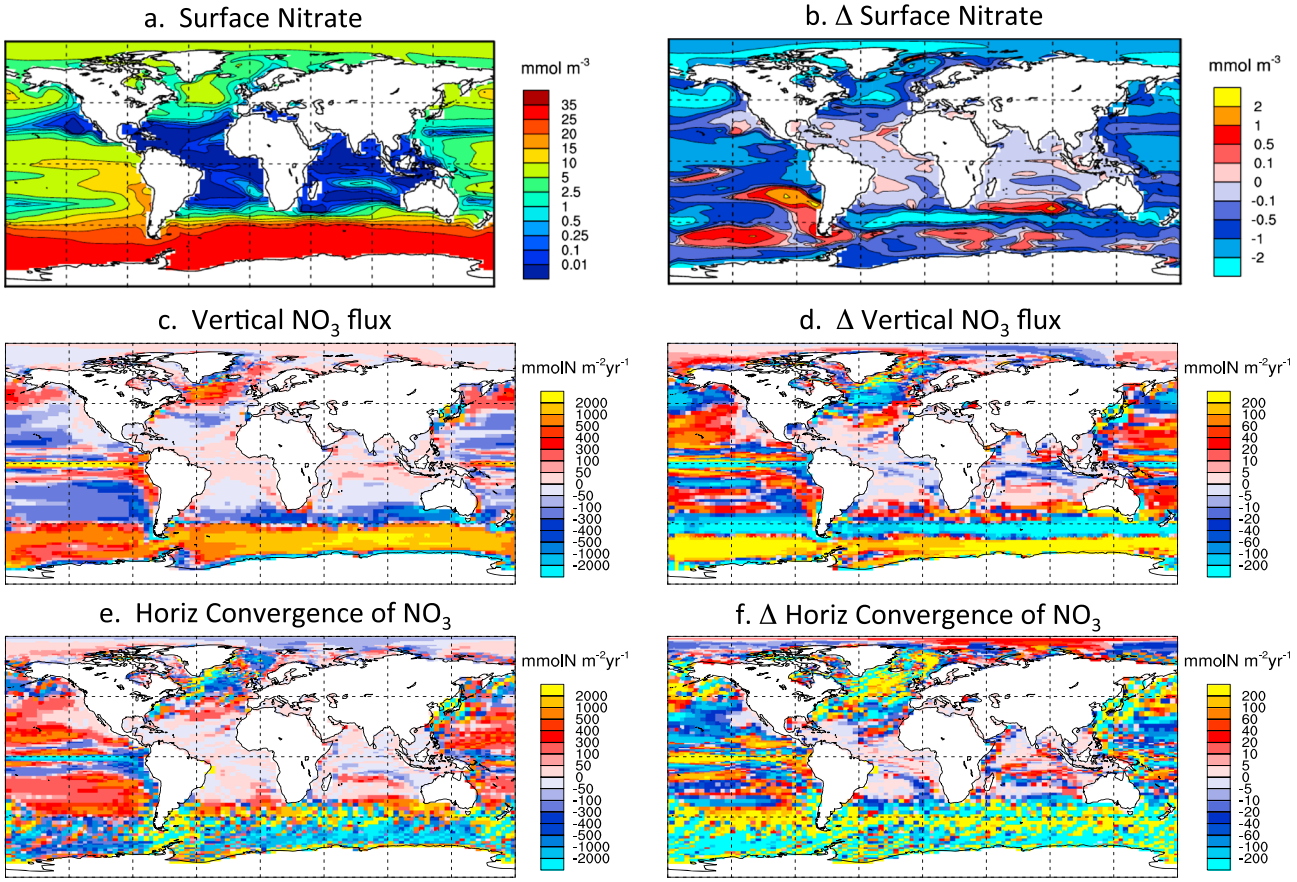

Figure 1. Global maps of the "present" values (average over years 1980–1999) and climate change signal (difference between years 1980–1999 and years 2080–2099) for (a and b) surface nitrate (mmol/m^3); (c and d) NO_3 vertical advection at the maximum annual MLD in mmol N/m^2/yr; and (e and f) NO_3 horizontal convergence vertically integrated up to the maximum annual MLD (mmol N/m^2/yr). These values were approximated off line from monthly nitrate and flow values.

prognostic variables include suspended and sinking particulate matter, dissolved inorganic carbon (DIC), alkalinity (Alk), oxygen (O_2), and dissolved nutrients: ammonia (NH_4), nitrate (NO_3), phosphate (PO_4), silicate (SiO_3), and iron (Fe). The model fixes the phytoplankton C/N/P ratios but allows for variations in Fe/C, Si/C, and chlorophyll to carbon (Chl/C) ratios depending on ambient nutrient and light availability. The parameterization of nitrogen fixation follows *Moore et al.* [2006].

[10] A thorough comparison of the ocean-only simulation output with observations was performed by *Doney et al.* [2009a, 2009b]. Coupled climate model spin-up includes a 1000 year preindustrial control simulation followed by a transient simulation for the 1870–2099 period [*Thornton et al.*, 2009]. Fossil fuel CO_2 emissions are prescribed from 1870–1999 historical data and from the SRES (Special Report on Emission Scenarios) A2 scenario for 2000–2099, corresponding to cumulative CO_2 emissions of 1855 GtC by year 2100 [*Solomon et al.*, 2007]. The time-evolving, simulated atmospheric CO_2 concentration is used in the atmospheric radiative transfer routines, and the land and ocean carbon sources/sinks respond to changes in simulated atmospheric CO_2, temperature, and climate. No other transient forcings (land-use change, variable iron deposition, anthropogenic aerosols, etc.) were applied to the simulations.

[11] The horizontal convergence of nitrate and iron by the mean flow and vertical nutrient fluxes at the maximum annual MLD were approximated off line from monthly mean model output (Figures 1 and S4). Since the eddy contributions and the vertical mixing coefficients were not saved for these model runs and cannot be recreated off line, we unfortunately cannot close the nutrient and biomass budgets. It is also unclear how different the climate driven changes in the off-line nutrient divergence terms are from the true terms calculated explicitly online. Hence, we only use here our offline nutrient flux calculations for qualitative visual guidance.

3. Results

[12] In th]e CCSM-3 model, diatoms do very well in nutrient-rich, high-latitude upwelling and frontal regions, and in the equatorial Pacific. The dominance of larger phytoplankton over small phytoplankton in nutrient-rich areas agrees with observations and is achieved in CCSM-3 through a weaker grazing pressure and slightly more efficient photoadaptation to low light (higher maximum Chl/N ratio) for diatoms compared to small phytoplankton, despite identical maximum specific growth rates for the two groups [*Moore et al.*, 2002, 2004]. Because of their lower nutrient half-saturation K coefficient, small phytoplankton outcompete diatoms in the well-stratified, well-lit, low-nutrient oligotrophic gyres, where they

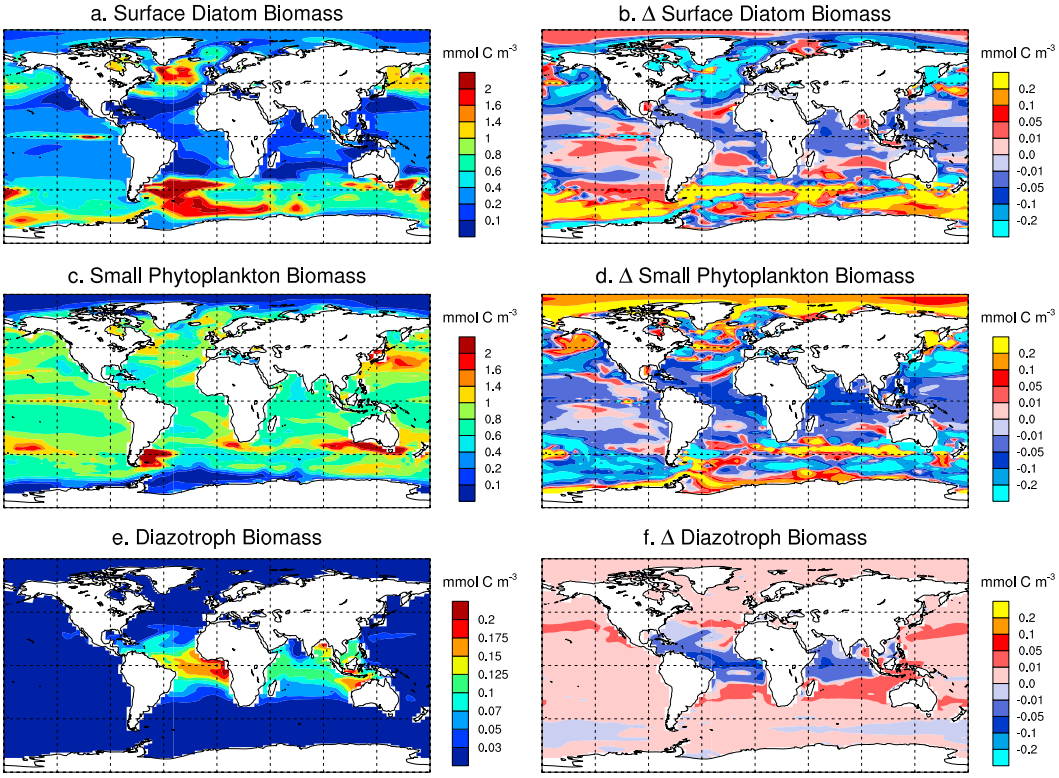

Figure 2. Global maps of the surface control values (average over years 1980–1999) and climate change signal (difference between years 1980–1999 and years 2080–2099) for (a and b) diatom biomass, (c and d) small phytoplankton biomass and (e and f) diazotroph biomass. Units are mmol C/m^3.

are efficiently grazed and the nutrients recycled (Figures 2a, 2c, and S1a).

[13] Iron-bearing dust originates primarily on continental deserts; larger distance from continental iron sources results in less aeolian iron flux to the ocean. Thus, iron is the main limiting nutrient for diatom and small phytoplankton growth in the Pacific and in all ocean basins south of 45°S, while nitrate is the main limiting nutrient in the Atlantic and Indian Oceans north of 45°S (Figure S2).

[14] The ecosystem composition—the relative contribution of each phytoplankton group to the total biomass—influences strongly total biological productivity and the efficiency of carbon export to the deep ocean.

[15] The export ratio (e-ratio) is the ratio between vertically sinking export flux, defined here as the downward flux of particulate organic matter at 100 m, and total biological production above that depth, and can be used as an indicator of the overall efficiency of carbon export to the deep ocean. The CCSM-3 model assumes that diatoms are preyed on by larger zooplankton and thus route a greater fraction of grazing to organic matter export rather than to remineralization, as previously observed [*Straile*, 1997]. Consequently, diatoms export carbon more efficiently to the deep ocean, while small phytoplankton are more efficiently recycled at the surface and export less organic matter to the deep ocean. Thus, high-latitude and upwelling regions where diatoms generally prosper are characterized by less recycling and a higher proportion of organic matter going to the sinking pool (i.e., higher e-ratios) compared to the oligotrophic low latitudes dominated by small phytoplankton (Figure 3e).

[16] The modeled ocean biogeochemistry and ecology patterns are different in the Southern compared to the Northern Hemisphere for the present climate (years 1980–1999). Compared to the NH biomes, SH biomes are generally characterized by deeper mixed layer depth and weaker stratification, resulting in more nutrient supply to surface waters. Higher-surface nutrients support higher diatom biomass, higher overall productivity, and higher $CaCO_3$ flux in the SH (except for the ice biome where this flux is negligible), as summarized in Table 1 (and the legends in Figure 4). Higher diatom biomass results, to a first order, in a larger and more efficient export production (i.e., larger e-ratio) in the Southern compared to the Northern Hemisphere in the present ocean (Table 1).

[17] The simulated physical response of the ocean to 21st century climate change is also different between the two hemispheres. The 21st century sea surface warming in the SH is slightly smaller than in the NH (Figure 4a), as previously observed in other climate modeling studies (see references in section 1). In agreement with previous studies [*Solomon et al.*, 2007], CCSM-3 predicts a stronger hydrological cycle, stronger seasonal cycle, more extensive sea ice retreat (Figure 4d) and land-ice melting in the NH; these factors all contribute to a stronger freshening of surface waters in the Northern compared to the Southern Hemisphere (Figure 4b). As a consequence of differential warming and freshening, the increase in water column stratification with climate change—observed both in the highly stratified low latitudes and the less stratified high latitudes—is more pronounced in the Northern than in the Southern Hemisphere (Figure 4c).

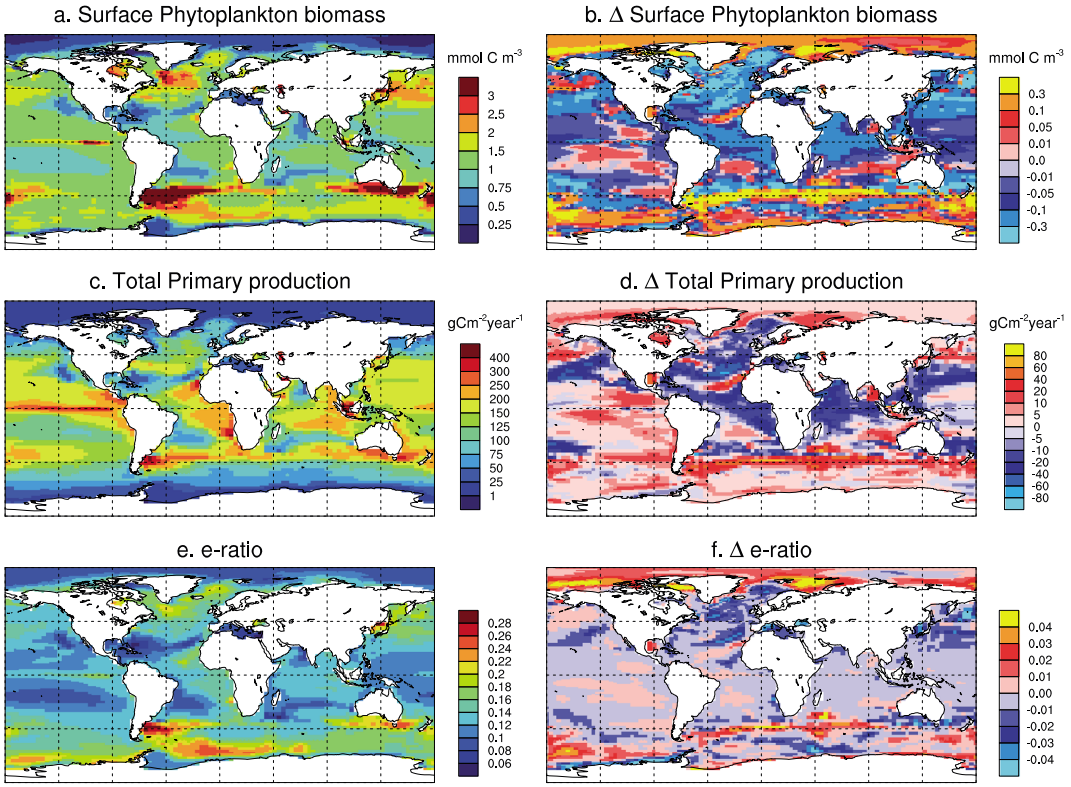

Figure 3. The control (1980–1999 average) and the response to climate change (calculated as difference from years 1980–1999 to 2080–2099) of the: (a and b) surface total phytoplankton biomass (mmol C/m^3), (c and d) total primary production (gC/m^2/yr), (e and f) export ratio defined as the ratio between export production at 102 m and primary production above this level (no units).

[18] Climate change results in a poleward shift and strengthening of the midlatitude westerlies (Figures 5a and 5b), in agreement with the latest generations of coupled models [*Yin*, 2005; *Barnes and Polvani*, 2013] and continuing the observed atmospheric trend over the past 50 years [*Swart and Fyfe*, 2012]. The poleward shift and intensification in westerlies result in increases in Ekman upwelling south of 45°S (Figures 5c and 5d) and increases in the maximum annual mixed layer depth (MLD) in the 30°S–55°S band (Figures 5e and 5f), consistent with mechanisms previously observed in this class of models [e.g., *Cai et al*., 2010; *Gent and Danabasoglu*, 2011]. The 21st century shift in westerlies is asymmetrical, with a much larger shift in the SH than in the NH, as also observed over the past 40 years. This asymmetry is partly due to the differential depletion of stratospheric ozone over Antarctica, which cools the stratosphere and increases the stratosphere-troposphere thermal contrast in the south more, helping intensify the southern westerlies [*Thompson and Solomon*, 2002]. Increased wind energy acts to destroy the vertical stratification of the ocean, contributing to the smaller net increase in stratification in the Southern compared to the Northern Hemispheres over the 21st century.

[19] Will physical triggers that are different in the two hemispheres also result in different climate-driven responses of biogeochemical cycling and phytoplankton ecology in the two hemispheres? To respond to this question, we next analyze in detail the ecological response to 21st century warming—and resulting North-South asymmetries—across the major ecological biomes: equatorial and low-latitude upwelling, subtropical, subpolar, and marginal sea ice. These ecological biomes are defined based on physical criteria, closely following the definitions employed by *Sarmiento et al*. [2004] and conceptually along the lines of *Longhurst* [1994]. Details of the ecological partitioning are in Appendix B. Climate change results in changes in the sizes of the various biomes, including a retreat of the ice biome and an expansion of the subtropics. These changes are discussed in the supporting information and shown in Supplementary Table 1. For our present analysis, we choose to focus on climate-driven changes in ocean ecology within fixed geographic biomes; we therefore assume the 1980–1999 average boundaries and sizes for our biomes as shown in Figure 6.

[20] Climate-driven changes in relevant biological, chemical, and physical indices are calculated within each of our fixed geographical biomes (Figure 7). The figure highlights the differences between the responses of equivalent SH biomes (in red) and NH biomes (in green) to 21st century climate change; these differences are discussed in detail in the following sections. Climate change modifies the net growth of phytoplankton via changes in both bottom-up factors (nutrients, light, temperature) and top-down factors (zooplankton grazing). Figure 8 shows climate-driven changes in each of these components across all (geographically fixed) major biomes, for the SH (red) and NH (green).

[21] Two results from our previous work [*Marinov et al*., 2010] are useful in our present analysis and can be confirmed by examining climate-driven changes in phytoplankton growth rates (Figures S1c and S1d). First, the *critical nutrient*

Table 1. Average Response of Model Ecology and Biogeochemistry to Global Warming in the 21st Century[a]

	Biome Area ($\times 10^{12}$ m^2)	Small Phytoplankton Biomass (mmol C/m^3)	Diatom Biomass (mmol C/m^3)	Total Phytoplankton Biomass (mmol C/m^3)	Zooplankton Carbon (mmol C/m^3)	Productivity Above 103 m (PgC/yr)	Export Production at 103 m (PgC/yr)	$CaCO_3$ Flux (PgC/yr)	e-ratio
Global	349.3	0.51(−3.1%)	0.37(−1.8%)	0.89(−2.4%)	0.39(−4.1%)	49.92 (−1.2%)	6.42(−2.8%)	0.44(−5.9%)	0.13(−1.9%)
NHem	142.9	0.51(−1.7%);	0.32(−10.5%)	0.85(−5.1%)	0.38(−5.9%)	21.05(−4.6%)	2.54(−8.4%)	0.18(−7.0%)	0.12(−3.7%)
SHem	206.4	0.51(−4.0%)	0.40(3.3%)	0.93(−0.7%)	0.39(−2.8%)	28.87(1.2%)	3.88(0.8%)	0.26(−5.2%)	0.13(−0.7%)
Subtropical NHem	67.3	0.59(−4.5%)	0.26(−15.1%)	0.86(−7.5%)	0.40(−9.4%)	10.00(−7.4%)	1.16(−11.6%)	0.09(−10.2%)	0.11(−4.2%)
Subtropical SHem	95.3	0.61(−3.3%)	0.37(0.9%)	1.00(−1.4%)	0.43(−2.9%)	14.42(1.5%)	1.91(0.6%)	0.14(−3.7%)	0.13(−0.6%)
Subpolar NHem	17.8	0.51(−0.5%)	0.46(−11.6%)	0.97(−5.6%)	0.43(−1.6%)	2.08(−2.6%)	0.30(−7.9%)	0.02(−6.2%)	0.13(−2.9%)
Subpolar SHem	36.5	0.48(−9.3%)	0.50(15.7%)	0.98(3.4%)	0.38(−0.6%)	4.09(6.9%)	0.64(10.3%)	0.05(−11.4%)	0.13(2.2%)
Ice NHem	15.1	0.20(38.2%)	0.24(−9.8%)	0.44(11.9%)	0.18(15.9%)	0.82(12.7%)	0.11(3.2%)	0.01(27.0%)	0.11(−3.9%)
Ice SHem	25	0.12(13.0%)	0.40(2.8%)	0.52(5.1%)	0.16(5.8%)	1.09(6.3%)	0.21(4.3%)	0.01(5.3%)	0.14(−4.2%)
LLU NHem	25.4	0.53(−4.2%)	0.35(−6.4%)	0.92(−5.2%)	0.42(−6.7%)	4.44(−3.7%)	0.55(−6.4%)	0.03(−5.6%)	0.12(−2.8%)
LLU SHem	32.3	0.54(−3.9%)	0.37(−4.1%)	0.93(−3.7%)	0.43(−5.4%)	5.78(−2.2%)	0.72(−5.0%)	0.04(−4.4%)	0.12(−2.9%)
Equatorial	34.6	0.51(−4.3%)	0.45(−4.2%)	0.99(−4.5%)	0.43(−6.3%)	7.10(−3.0%)	0.83(−5.0%)	0.05(−5.8%)	0.12(−2.0%)

[a]For each variable and biome, we show the mean 1980–1999 value and the fractional change from 1980–1999 to 2080–2099 (in parenthesis). Variables are in order: biome areas ($\times 10^{12}$ m^2) defined as in Appendix B, small phytoplankton carbon (mmolC/m^3), diatom carbon (mmolC/m^3), total phytoplankton carbon (mmolC/m^3), zooplankton carbon (mmolC/m^3), total productivity integrated over the biome (PgC/yr), export production (particulate organic carbon or POC flux) at 103 m integrated over the biome (PgC/yr), $CaCO_3$ flux at 103 m (Pg C/yr), e-ratio (calculated as POC flux at 103 m divided by the integral of primary production above 103 m). Biomass carbon values are averages over top 103 m. Ecological biomes are in order: Global ocean, Northern Hemisphere, Southern Hemisphere, Northern subtropical, Southern subtropical, Northern subpolar, Southern subpolar, Northern sea ice biome, Southern sea ice biome, Northern low-latitude upwelling, Southern low-latitude upwelling, Equatorial biome. For all our calculations we define the biomes as averages over years 1980–1999 as shown in Figure 6.

hypothesis suggests that model diatoms (small phytoplankton) will respond more to changes in nutrient in high nutrient, high latitudes (lower nutrient, low latitudes). Secondly, *changes in light and temperature affect preferentially smaller phytoplankton* in all ocean biomes. Our model assumes a multiplicative growth equation of nutrients, temperature and light (equation (A2)), identical temperature dependence of growth for small and large phytoplankton and the *Geider et al.* [1998] formalism for light limitation. In this framework, differential phytoplankton responses to changing light and temperature are indirectly driven by interspecies difference in the nutrient functional response terms V_x and hence by differences in the nutrient half-saturation rates (see equations (A6a), (A6c), (A3), and (A4)). Since smaller phytoplankton have lower half-saturation coefficients, they have larger nutrient functional responses and they will thus respond more to changes in light and temperature than diatoms anywhere in the ocean.

3.1. Equatorial and Low-Latitude Upwelling Biomes

[22] In the present day ocean (years 1980–1999 in our simulation), the equatorial and low-latitude upwelling (LLU) biomes account for 26.4% of the total area, 28% (27%) of the total diatom (small phytoplankton) biomass, and 34.7% of the global ocean productivity (Table 1). In these low-latitude biomes, small phytoplankton and diatoms are limited by iron in the Pacific basin and by nitrogen in the Indian and Atlantic basins.

[23] Twenty-first century climate change results in a patchy nutrient supply response, with decreased vertical velocity and mixed layer depth decreasing vertical nitrate and phosphate supply to the surface in the low-latitude Atlantic and Indian basins (Figure 1). In turn, decreased nutrient supply drives decreases in both small phytoplankton and diatom growth rates, biomass, and primary production in the globally integrated LLU biomes and equatorial biome, with larger nutrient-driven decreases in the Northern compared to the Southern LLU zones (Figures 7e and 8e). Analysis of phytoplankton growth rates (Figure 8e) and a separate statistical trend analysis (Figure S3) confirm that the decreasing trend in diatom biomass in the Atlantic, Indian, and West Pacific basin low-latitude equatorial and LLU biomes is nutrient driven. In contrast to these regions and the biome mean, we notice an increase in phytoplankton biomass and total primary production in the East Pacific low latitudes (~135°W to 90°W). Interestingly, this regional increase in biological production happens despite small decreases in the vertical Fe supply (Figure S4) and incident light supply (Figures 9b and 9d) and is due to the surface temperature increase directly affecting the growth rate of phytoplankton.

[24] In CCSM-3, temperature-limited diazotrophs are found primarily in the LLU and Equatorial biomes of the Atlantic and Indian Oceans, with lower concentrations (0.01 mg Chl/m^3) everywhere else in the 40°S–40°N band (Figure 2e). Since they fix all the nitrogen they need from N_2 gas, diazotrophs are limited by either iron or phosphate. Climate change results in a reduction in the vertical supply of PO_4 to the mixed layer and hence a switch from iron to phosphate limitation of diazotrophs in the South Atlantic and South Indian equatorial and low-latitude upwelling biomes (Figure S2). Decreased mixed layer phosphate results in an overall decrease in (phosphate limited) diazotroph biomass and nitrogen fixation in the Indian and Atlantic

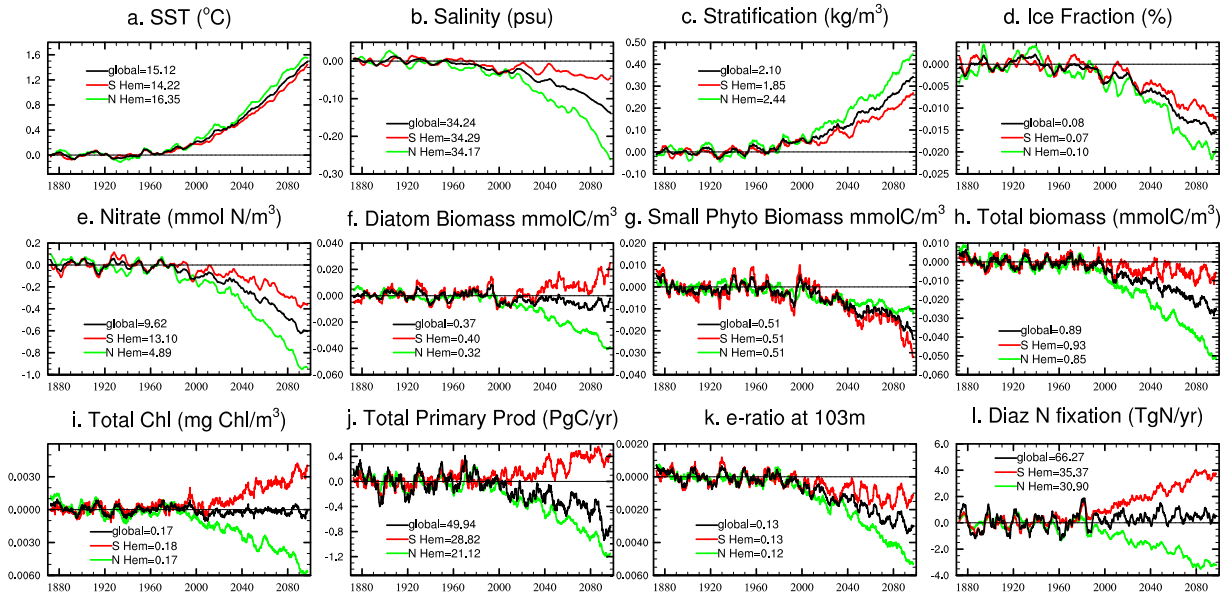

Figure 4. (a) Time series of globally integrated sea temperature change (°C) from 1870 to 2100 for the Northern Hemisphere (green), Southern Hemisphere (red), and global average (black). Plotted is the deviation from the 1870–1959 mean, which is shown in the horizontal black line and in the legend for each plot. Same as above for (b) salinity (psu), (c) stratification (kg/m^3) defined as surface minus 200 m density, (d) fractional ice cover (% area), (e) nitrate (mmol/m^3), (f) diatom biomass (mmolC/m^3), (g) small phytoplankton biomass (mmolC/m^3), (h) total phytoplankton biomass (mmolC/m^3), (i) total chlorophyll (mg Chl/m^3), (j) total primary production integrated over the top 102 m (PgC/yr), (k) e-ratio defined as the ratio between export production at 102 m and primary production above this level (no units), (l) diazotroph nitrogen fixation (Tg N/yr). All values are column averages over the top 102 m unless otherwise indicated.

basins north of ~10°S. By contrast, increased iron supply in the SH winter and spring results in an increase in (iron limited) diazotroph biomass and nitrogen fixation in the 10°S–40°S band over the 21st century (Figure 2f). In the global average, the SH increase and NH decrease in diazotrophs compensate, resulting in no significant climate-driven change in total global diazotroph biomass or nitrogen fixation (Figure 4l).

3.2. Subtropics

[25] This biome has critical relevance for global ocean biology, accounting in the CCSM-3 simulation for 48% of the global ocean chlorophyll and primary production, 55% of the small phytoplankton global biomass, and 41% of global diatom biomass. Importantly, while covering only 47% of the total ocean area, the subtropics account for 84% of the decrease in globally integrated primary production and 76% of the decrease in total phytoplankton biomass observed in CCSM-3 over the 21st century. Small phytoplankton dominate over diatoms and account for most of the biological production in this regime (Table 1). Small phytoplankton compete better in more stratified waters with lower background nutrients. This explains their higher relative abundance in the subtropical North Atlantic (64% of total chlorophyll) compared to the subtropical South Atlantic (52%), and generally in the northern subtropics (63%) compared to the southern subtropical biomes (58%). Export ratios reflect the underlying ecosystem composition; more small phytoplankton relative to diatoms result in a lower e-ratio in the North Atlantic (0.11) compared to the South Atlantic (0.14).

[26] We note the high similarity between the climate-driven changes in phytoplankton biomass and nutrient limitation term (compare Figures 2b and 9b). Nutrient limitation is more significant than light limitation for phytoplankton growth in this regime, as shown by the tight positive 120 year temporal correlations between biomass and nutrient limitation and the weaker biomass-light correlations (Figures 9e and 9f). Small phytoplankton and diatoms decrease over the 21st century in the NH subtropics by 4.5% and 15%, respectively, and most of this trend can be explained by the decrease in nutrients, as indicated by growth rate analyses (Figure 8b) and statistical trend analysis (Figure S3). The relevant question for us then becomes: How are nutrients supplied to the subtropics and why is there a decrease in nutrient supplies over the 21st century?

[27] Subtropical gyres are characterized by lateral convergence of surface flow, nutrients, and phytoplankton biomass (Figures 1e and S4e). Nutrients above the seasonal boundary layer in the subtropics are supplied via lateral convergence and diffusive vertical supply into the mixed layer and are lost by vertical advection out of the surface or by photosynthesis and subsequent export of organic matter via sinking particles. The lateral convergence of nutrients in these biomes is dominated by large values at the subpolar-subtropical boundaries indicating a subpolar source of nutrients (Figure 1e) [see also, e.g., *Williams and Follows*, 1998; *McGillicuddy et al.*, 2003]. Isopycnal mixing and wintertime convective mixing were also shown to be important in maintaining the observed nutrient values and export fluxes in the subtropics [e.g., *Williams et al.*, 2000].

[28] Decreases in maximum annual MLD (Figure 5f) over parts of the subtropics might indicate decreased vertical diffusive supply and seasonal convective transport of nutrients to the

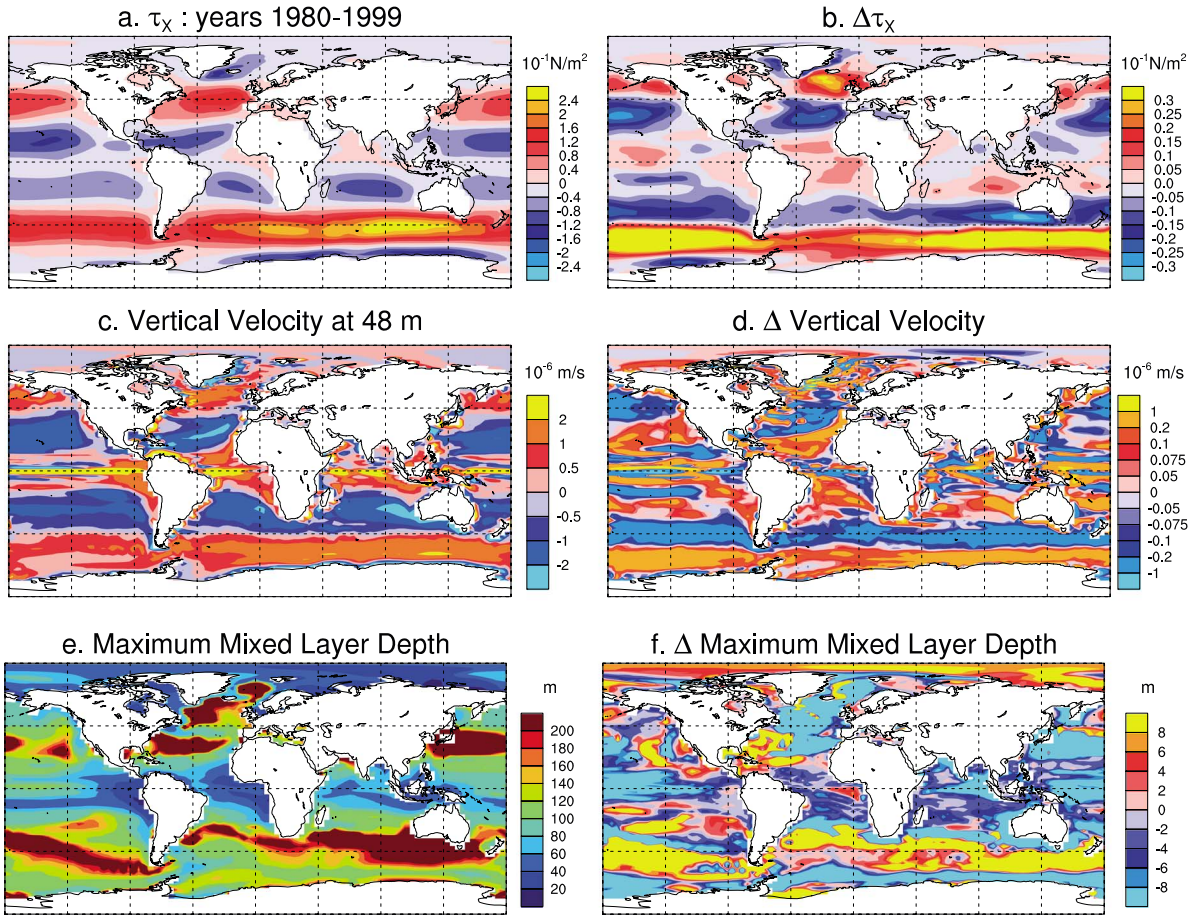

Figure 5. (a and b) Horizontal wind stress averaged over 1980–1999 and the change in wind stress between 2080–2099 and 1980–1999 (10^{-1} N/m^2). Same as above for (c and d) the vertical velocity in the ocean model at 48 m depth (10^{-6} m/s) and (e and f) maximum annual mixed layer depth (m).

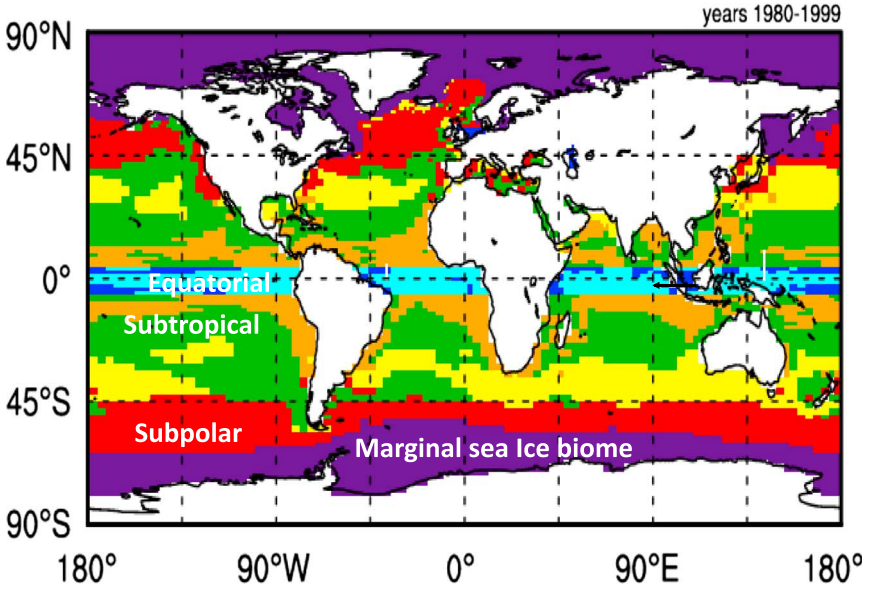

Figure 6. Ecological Biomes in the model, calculated for 1980–1999. Illustrated are the Equatorial biome (light blue: upwelling; dark blue: downwelling), low-latitude upwelling (orange), permanently stratified subtropical (yellow), seasonally stratified subtropical (green), subpolar (red), and marginal sea ice (purple) biomes, as defined in Appendix B. The sizes of these biomes are shown in Table 1.

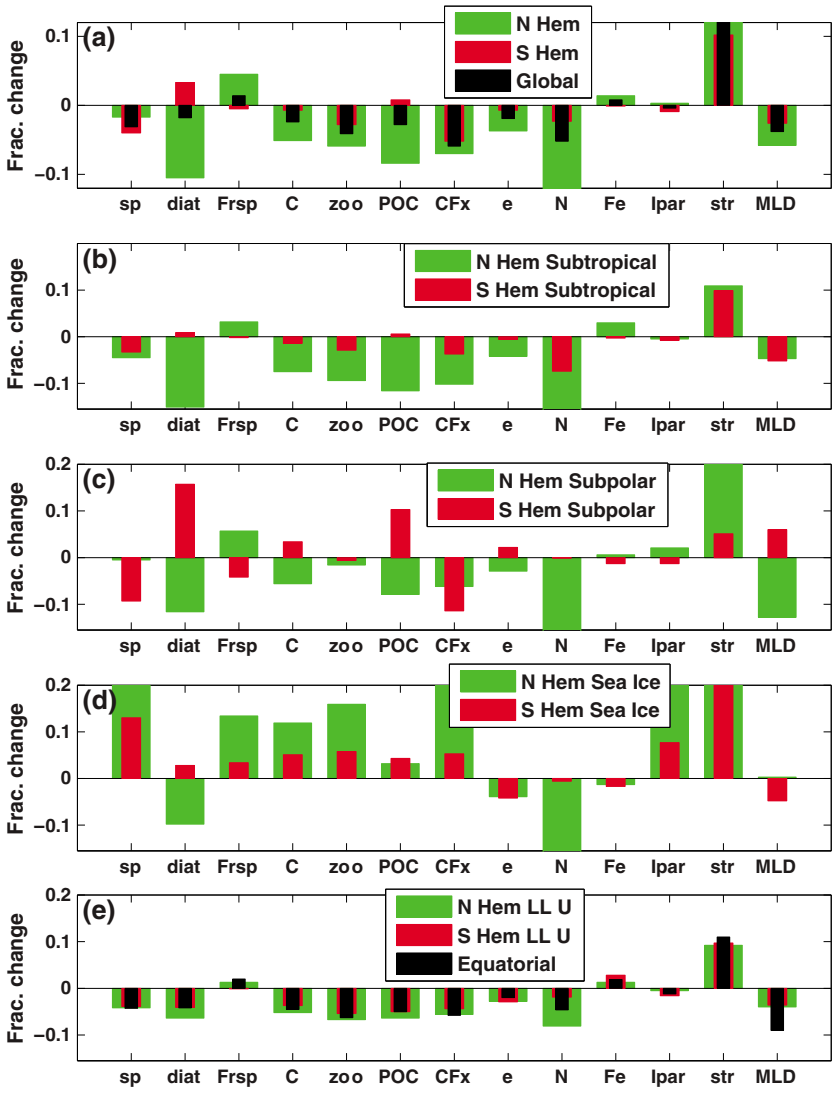

Figure 7. Annually averaged ecological-biogeochemical responses to climate change. The fractional changes in variables from 1980–1999 to 2080–2099 for the (a) Northern Hemisphere (green) and Southern Hemisphere (red) and global (black) values, (b) Northern/Southern Hemisphere subtropics, (c) Northern/Southern Hemisphere subpolar, (d) northern/southern marginal sea ice, (e) northern/southern low-latitude upwelling and Equatorial biomes. Variables are from left to right: small phytoplankton and diatom biomass, relative abundance of small phytoplankton (small divided by total phytoplankton biomass), total phytoplankton biomass, zooplankton biomass, POC flux (export production) at 103 m, $CaCO_3$ flux (CFx) at 103 m, e-ratio (calculated as POC flux at 103 m divided by primary production integrated above 103 m), NO_3, Fe, I_{par}, stratification (density difference between surface and 200 m), mixed layer depth. Values represent averages over top 103 m of the watercolumn for all phytoplankton and zooplankton biomass, relative abundance, nutrients, and I_{par}. 0.1 represents a 10% fractional change.

surface. We posit that decreased upwelling and vertical nutrient supply decrease strongly the limiting nutrient concentrations in surface waters of subpolar regions and contribute to a drop in the lateral nutrient supply to the subtropics over the 21st century (Figures 1b, 1d, and 1f). The decreased lateral convergence of flow and nutrients into the subtropics (Figure 1f) might also be associated with a slowdown of the Northern subtropical gyres over the 21st century. Changes in gyre circulation, as well as changes in the seasonal convergence of nutrients and isopycnal nutrient supply differ in the Northern and Southern subtropics.

[29] The typical subtropical behavior is seen in the North Atlantic subtropics. Here climate change does not change much the wintertime light limitation but strongly decreases the summer nitrate supply and consequently both small phytoplankton and diatom biomass. Diatoms ($r = 0.71$) are better correlated with nutrient limitation compared to small phytoplankton ($r = 0.39$), as seen in Figure 9e. This behavior is likely due to the much weaker control of grazers on diatoms than on small phytoplankton, which allows diatoms to responding strongly to nutrient fluctuations in the environment.

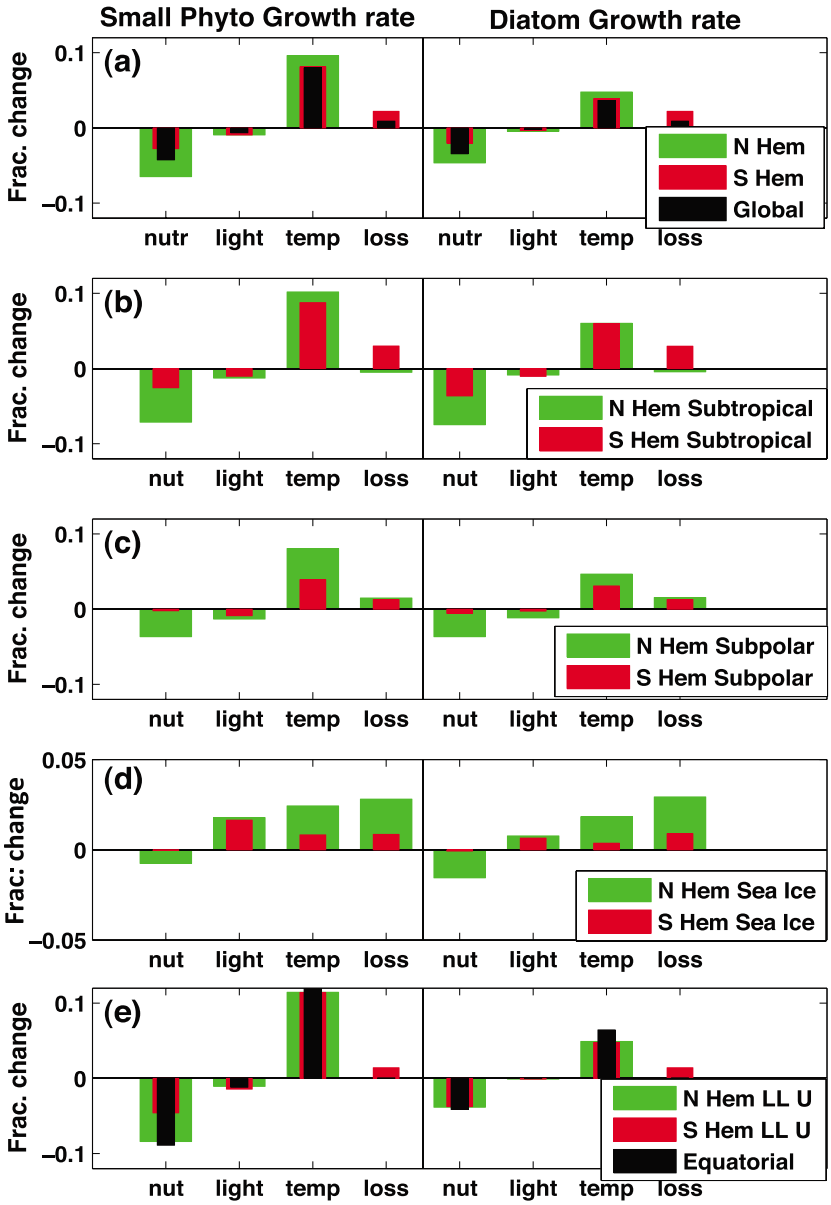

Figure 8. Annually averaged ecological-biogeochemical responses to climate change for the various biomes, as in Figure 7. Variables shown are nutrient, light, and temperature contributions to the 1980–2100 trend in surface phytoplankton specific growth rate ($\Delta\mu_x^{nutr}$, $\Delta\mu_x^{light}$, $\Delta\mu_x^{temp}$) as calculated from equations (A6a), (A6b), (A6c); as well as the phytoplankton loss rate (sum of grazing, linear loss, and aggregation rate, in day^{-1}). All variables shown for both small phytoplankton and for diatoms. Northern Hemisphere biomes in green, Southern Hemisphere biomes in red.

[30] The climate change response pattern of phytoplankton biomass is patchy in the SH subtropics. We note smaller decreases in limiting nutrients than in the Northern subtropics and locally even increases in the limiting nutrients (e.g., increased patches of nitrate and iron in the East South Pacific, localized increases in nitrate in the Western South Atlantic and Western South Indian subtropical gyres, Figures 1b and S4b). Localized increases in nutrients, together with increased temperatures (Figures 9b and 9c) result in localized increases in diatom and small phytoplankton growth rates and biomass at these locations (Figure 2b). An analysis of growth rate terms shows that the temperature increase dominates over the small decrease in nutrients in the biome average, such that SH subtropical diatom productivity and biomass increase slightly overall with climate change (Figures 8b and 7b). By contrast, small phytoplankton biomass decreases in this biome despite an increase in small phytoplankton productivity. This reflects a tight grazing control on small phytoplankton biomass: as temperature increases, grazing of small phytoplankton also increases, compensating much of the direct temperature driven growth rate increase. In summary, in the SH subtropical biome diatoms become relatively more competitive with climate change, with slight (1–2.2%) increases in diatom chlorophyll and production in the South Atlantic and Pacific subtropics, and more significant (9%) increases in diatom chlorophyll and production in the South

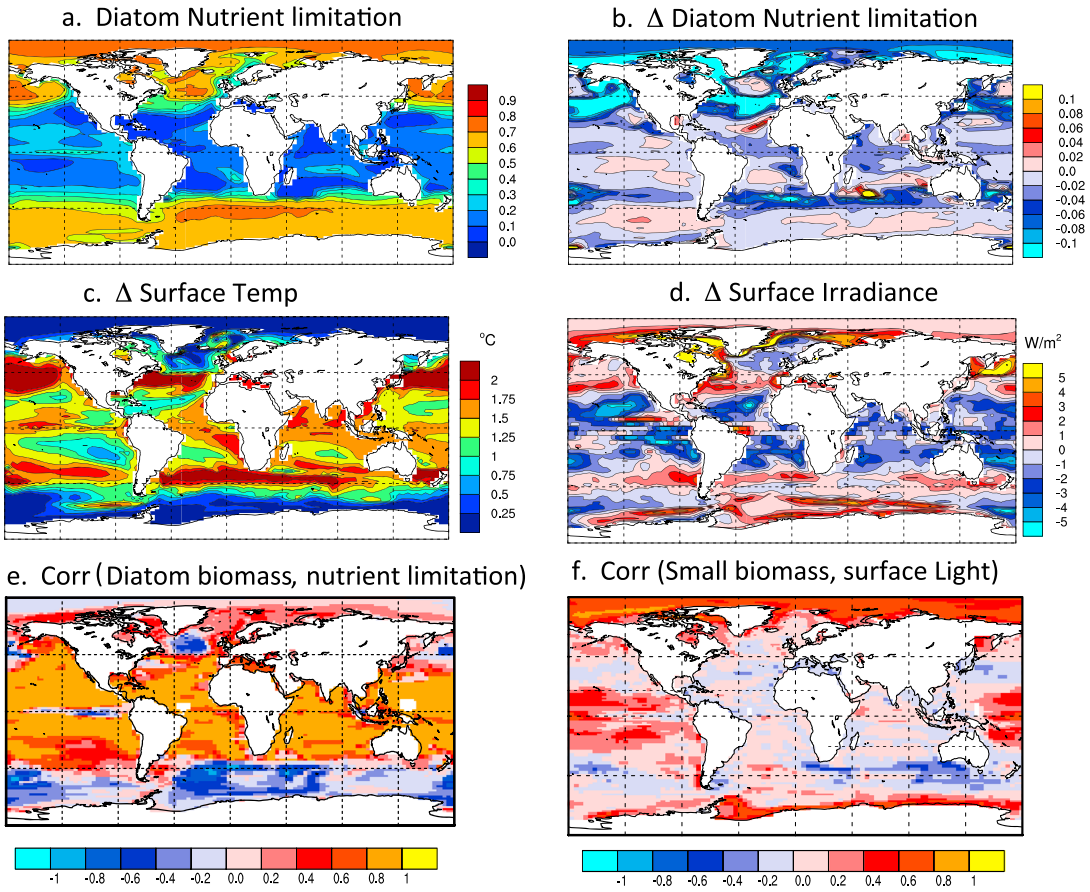

Figure 9. (a) The control (1980–1999 average) diatom nutrient limitation, calculated from equation (A3) in the text. The response to climate change (calculated as difference from years 1980–1999 to 2080–2099) of the: (b) diatom nutrient limitation, (c) surface temperature, (d) surface light. The 100 year monthly temporal correlations between: (e) diatom biomass and diatom nutrient limitation and (f) small phytoplankton biomass and surface light.

Indian subtropics. There is no change in export production in the Southern subtropics and only a 1% increase in total production and a 1% decrease in the e-ratio.

[31] The projected subtropical biome response to climate change can be summarized as follows:

[32] 1. Phytoplankton biomass, zooplankton, primary production, particulate organic carbon export fluxes, and carbonate fluxes decrease in the globally averaged subtropical biome (Figure 7b) and are responsible for globally averaged decreases in these indicators (Figure 7a). These changes are primarily due to decreases in small phytoplankton and diatoms in the NH subtropics, in turn driven by drops in vertical and horizontal nutrient supplies to the surface ocean.

[33] 2. Diatoms have opposite responses in the two hemispheres: large nutrient driven decrease in the NH subtropics and a small temperature driven increase in the SH subtropics.

[34] 3. Increasing nutrient limitation results in average decreases in the export flux of organic matter at 100 m in the NH subtropics by about 10% over the 21st century but no equivalent changes in the SH subtropics (Figure 7b). A decrease in the export ratio of 4% in the subtropics reflects a stronger decrease in export production compared to the decrease in total production, in agreement with a decreasing (increasing) relative role of diatoms (small phytoplankton) in the system and a transition to a lower biomass, more oligotrophic, more efficiently recycled system. This transition to a more oligotrophic system is much clearer in the Northern compared to the Southern subtropical biome, where there are minimal changes in the e-ratio (Figure 7b).

3.3. The Subpolar Biome and the Subpolar-Subtropical Boundary

[35] The subpolar domain in the CCSM-3 simulation accounts for 15.5% of the global ocean area, 12% of the global primary production, and 15% (20%) of the global ocean small phytoplankton (diatom) biomass. Changes in temperature, grazing, nutrients, and light combine to give us strikingly different ecological responses in the NH and SH subpolar biomes. Notable observations include:

[36] 1. A pronounced increase in diatom, total biomass, total primary production, and e-ratio at the Southern Ocean subtropical-subpolar boundary (Figures 2b, 3b, 3d, and 3f).

[37] The subtropical-subpolar boundary is the boundary between the warm and salty thermocline waters of the subtropical gyres and the colder, fresher subpolar regime and is represented in our model by a discontinuity in surface temperature and salinity (of ~5°C and 0.5 psu, respectively) at about 40°S. This boundary is maintained through mechanical and

thermal forcing by the surface westerlies and corresponds approximately to the zero surface wind stress curl, and thus roughly coincides with the subtropical front in the real ocean. This boundary marks the transition between nitrogen and iron limitation of phytoplankton in the Atlantic and Indian Oceans (Figure S2) and is the site of the principal diatom blooms in the ocean model. While diatom growth rate peaks broadly between 50°S and 35°S, lateral advection acts to concentrate the maximum diatom biomass, total ocean primary production, and export in the model at 40°S–45°S, coincident with the front (Figures 2b, 3c,and 3e).

[38] Over the 21st century, the southward shift and intensification of the maximum westerlies result in a global average southward shift of a few degrees in the subtropical-subpolar boundary and an enhanced northward Ekman transport of water and heat from south of 50°S (as shown by *Cai et al*., 2010). The enhanced warming in the vicinity the subtropical-subpolar boundary and more broadly in the 35°S–50°S band (Figure 9c) is partly due to this wind mechanism and has been observed by others [e.g., *Capotondi et al*., 2012; *Sen Gupta et al*., 2009; *Cai et al*., 2010] and nicely coincides with a band of increased total biomass and productivity. Additionally, increased westerlies result in increased convergence of biomass in the 40°S–55°S band (Figure S1). As we are in an area where diatoms abound, the increase in the northward transport of biomass in this band is more significant for diatoms than for small phytoplankton (Figures S1e–S1f). We suggest that a combination of increased temperature, preferential grazing of small phytoplankton over diatoms, and northward transport of biomass act to increase diatom biomass and production, as well as total biomass, productivity, and e-ratio preferentially at the 40°S–50°S subpolar-subtropical boundary (Figures 2b, 3b, 3d, 3f).

[39] 2. Southern Ocean subpolar biome total biomass, productivity, and e-ratio increase with climate change, a signal driven by a 15% increase in diatoms. Small phytoplankton decrease by 9%.

[40] Increasing winds and upwelling increase vertical Fe supply to the mixed layer in the Southern Ocean south of 50°S but also increase horizontal loss of nutrients via increased horizontal divergence of Fe (Figure S4). Increased cloudiness and increased MLD (Figure 5f) result in a decrease in the amount of light available for photosynthesis in spring and summer. In the SH subpolar biomes diatom growth, biomass and production increase because of localized increases in Fe south of 50°S combined with temperature increases, compensated somewhat by increased grazing and decreased light (Figure 8c). As previously discussed, decreasing light preferentially limits small phytoplankton growth; hence, we see large summer decreases in small pythoplankton biomass, relative abundance, primary production, and $CaCO_3$ flux of more than 15% in both the South Atlantic and South Pacific subpolar biomes, with more modest decreases in the fall and spring. The 16% increase in diatoms wins over the 9% decrease in small phytoplankton biomass, such that total phytoplankton biomass, primary, and export production, increase by 8–10% in the Subpolar Southern Ocean as a whole. The significant increase in diatoms makes this the only biome where the e-ratio increases with climate change (by 30% in the South Atlantic, 7% in the South Pacific, 11% in the South Indian; see also Figure 7c), signaling a more efficient organic matter export to the deep ocean.

[41] 3. Northern Hemisphere subpolar total phytoplankton biomass, productivity, and export ratio decrease with climate change; a signal driven by a 12% decline in diatoms.

[42] On average, temperature increases are larger in the NH compared to the SH subpolar biome; hence, the temperature driven increases in growth rates are larger in the NH subpolar biomes than in the SH subpolar biome for both small and large phytoplankton (Figure 8c). Since temperature preferentially impacts small phytoplankton growth in CCSM-3, the temperature-driven growth rate increase calculated from equation (A6c) is larger for small phytoplankton than for diatoms (Figure 8c). However, grazing acts to differentially keep in check the small phytoplankton and increases with increasing temperature, cancelling some of the temperature-driven phytoplankton growth.

[43] The growing stratification of the water column over the 21st century has a direct impact on vertical entrainment, which is responsible for most of the resupply of surface nutrients in the subpolar biomes. We estimate a decrease in the vertical nitrate flux into the base of the seasonal thermocline in the subpolar North Atlantic and North Pacific and a drop in the vertical Fe flux in the subpolar North Pacific (Figures 1 and S4), resulting in considerable decreases in nutrients and nutrient driven decreases in small phytoplankton and diatom growth rates in the Northern subpolar biome (Figure 8c).

[44] In the NH subpolar biome, a large decrease in nutrients dominates over the temperature increase and acts to decrease phytoplankton. In agreement with the critical nutrient hypothesis [*Marinov et al*., 2010], nitrate decrease preferentially decreases diatoms over small phytoplankton in this high nutrient region (e.g., Figure S1c). The opal and POC flux, total production and export ratio all decrease in the Northern subpolar biome as they are tightly correlated with diatom carbon (correlation coefficient > 0.7), signaling increased recycling and reduced export production, i.e., a less efficient carbon transport to the deep ocean (Figure 7c). Small phytoplankton changes minimally in this biome, indicating a compensation between nutrient-driven decreases and temperature and light-driven increases.

3.4. The Marginal Sea Ice Biome

[45] In CCSM-3, marginal sea ice biomes account for 11.5% of the global surface area, 10.5% of the diatom biomass, 3.4% of the small phytoplankton biomass, and 3.8% of the total productivity. In the marginal sea ice biomes, diatoms and small phytoplankton bloom in the spring and summer when light is sufficient; while nutrient limitation is most important for growth during the summer. A climate-driven increase in stratification, a decrease in sea ice cover and a shoaling in the SH ice biome mixed layer depth are responsible for both a decrease in limiting nutrients (nitrate in the northern sea ice biome or iron in the southern sea ice biome) and an increase in light availability for phytoplankton. We discuss each of these mechanisms below and point out that North-South differences in the response of stratification and light to climate change result in large North-South differences in ecology.

[46] During the summer months, the increase in stratification under climate change is almost twice as strong in the NH compared to the SH sea ice biomes, due to (a) higher temperature increase, a stronger seasonal cycle and stronger freshening in the Northern biome and (b) higher winds in the Southern sea ice biome countering the increasing stratification. This results in a much more pronounced fractional decrease in

limiting nutrients during summer-fall in the NH compared to the SH biome; a decrease in nitrate is the primary driver for the long-term diatom decrease in the NH sea ice biome (Figure 7d). In agreement with the critical nutrient hypothesis [*Marinov et al*., 2010], since this is a high nutrient biome, nitrate decrease preferentially decreases diatoms over small phytoplankton, as reflected by the nutrient-driven growth rates in the NH sea ice biome (Figure 8d and also Figure S1c). By contrast, iron and therefore nutrient-driven phytoplankton growth rates change minimally in the SH sea ice biome average, reflecting a compensation between wind-driven increases in the vertical Fe upwelling and horizontal divergence of Fe (Figure S4).

[47] Increases in light availability and temperature preferentially increase small phytoplankton over diatom growth (Figure 8d and also Figure S1d), acting to increase small phytoplankton in both the NH and SH sea ice biomes. Increases in small phytoplankton growth are strongest in the NH sea ice biome, with a well-defined increase in June–September and a poleward shift in the summer peak. More modest increases in temperature and surface light (associated with less sea ice melting in the south compared to the north) imply more modest increases in small phytoplankton in the SH marginal ice biome.

[48] As a consequence of the above climate-driven mechanisms, in the Northern marginal sea ice biome diatoms decrease by 9.8% and small phytoplankton increase by 38%, while in the Southern sea ice biome small phytoplankton increase more than diatoms (13% versus 2.8%) (Figure 7d). Consequently, in both northern and southern sea ice biomes the relative abundance of small phytoplankton increases relative to that of diatoms and the e-ratio decreases, suggesting a decrease in the efficiency of carbon export to the deep and increased surface recycling. The increase in small phytoplankton is responsible for the increases in total biomass, production, and zooplankton, with all trends more pronounced in the Northern compared to the Southern sea ice biomes (Figure 7d).

4. Summary and Implications for Export Production

[49] In the model, we noticed consistent differences between Northern and Southern Hemisphere ecological responses to climate change across all biomes, as summarized in Figures 4 and 7 and Table 1:

[50] 1. A (biome averaged) decrease occurs in small phytoplankton and diatom biomass in the *low-latitude upwelling and equatorial biomes* in both hemispheres. The decrease is strongest in the NH biomes in agreement with a stronger enhancement of stratification, reduced mixed-layer depth, and a larger decrease in nutrient supply in this hemisphere (Table 1 and Figures 7e and 8e). While diazotroph biomass does not change in the global average, there are pronounced regional differences, with average increases (decreases) in the Southern (Northern) Hemispheric averages (Figure 4l).

[51] 2. Both diatom and small phytoplankton carbon decrease in the *Northern hemisphere subtropical biomes* due to increasing stratification and decreasing nutrient supply. This contrasts with the minimal decrease in biomass and production in the *Southern subtropics* due to a smaller drop in nutrient supply compared to the Northern subtropics (Figure 7b).

[52] 3. A small net increase is found in diatom and total phytoplankton biomass in the *Southern Hemisphere subpolar biome*, driven by a southward shift in the subpolar-subtropical boundary and related temperature driven growth increases, as well as localized Fe increases south of 50°S. By contrast, a decrease in diatom and total biomass due to reduced vertical nutrient supply is observed in the *Northern subpolar biome* (Figure 7c).

[53] 4. An increase in total phytoplankton biomass, chlorophyll, and productivity occurs in the *marginal ice zone* due to increasing temperatures and light availability and longer growing season for small phytoplankton. Small phytoplankton are increasingly favored over diatoms in marginal sea ice biomes; this tendency is stronger in the NH than in the SH (Figure 7d). This tendency agrees with the small phytoplankton responding more than diatoms to light and temperature increases everywhere in the CCSM-3 model, as we have shown analytically [*Marinov et al*., 2010].

[54] Averaged over the globe and by hemisphere, the responses of ocean biogeochemistry and ecology to climate change are governed by the nutrient limited low and midlatitude biomes. In these biomes (LLU, equatorial, and subtropical) and hence in the global average, climate warming results in increased stratification, a reduction in the supply of nitrate to the surface ocean and thus a drop in surface nitrate, and a global decrease in total phytoplankton biomass and productivity. Consistent with a larger increase in stratification, the reduction in the supply of subsurface nitrate to the surface is more dramatic in the NH compared to the SH (Figures 4c and 4e). The decrease in nitrate supply is primarily responsible for the decreases in total biomass, total primary, and export production in the NH (Figures 4h and 4j).

[55] Over the 21st century, total phytoplankton biomass shows little (<1%) change in the SH average, and a 5% decrease in the NH average from year 1990 onward (Figure 4h). Phytoplankton photoadaptation explains the difference in total phytoplankton carbon and chlorophyll patterns (Figures 4h and 4i). Increasing cloudiness and decreasing light increases the Chl/C ratio and hence total chlorophyll in the SH from year 2000 onward. Changes in the NH and SH chlorophyll compensate, such that the total global chlorophyll shows almost no change over time, while total biomass and primary production decrease (Figures 4h and 4j).

[56] The contribution of diatoms to primary production decreases globally by 2.6% over the 21st century. In the mixed layer, diatom fractional abundance decreases globally from 0.42 to 0.37, with a corresponding increase in small phytoplankton fractional abundance, over the 21st century for a tripling of atmospheric CO_2. For comparison, *Bopp et al*. [2005] noticed a global decrease in diatom fractional abundance of 0.27 to 0.24 for a quadrupling of atmospheric CO_2. Climate-driven changes in ecosystem structure result in changes in the efficiency of carbon export to the deep ocean. Globally, fewer diatoms relative to small phytoplankton contribute to a decrease in the e-ratio, indicating a decrease in the percent of organic matter exported to depth versus that which is remineralized at the surface. This implies a global transition to a slightly more oligotrophic system with lower biomass and more efficient recycling of nutrients in the euphotic layer.

[57] The globally averaged trends in export production show clear North-South differences (Table 1). The change in

ecosystem composition ensures that export production, which is disproportionately driven by large diatoms, decreases by 8% in the NH where most decrease in diatom abundance happens, and increases by 0.8% in the SH (where diatoms increase on average) over the 21st century. The result is a 2.8% decrease in global export production. Time series of the e-ratio (Figure 4k) confirm that the increase in oligotrophy (as measured by the decrease in e-ratio) is more pronounced in the NH. The subpolar Southern Ocean stands out in the global e-ratio maps (Figures 3e and 3f). In contrast to most other ocean regions, the increased abundance of diatoms in the subpolar Southern Ocean results in an increase in the e-ratio, indicating a more efficient export of organic matter to the deep ocean under future warming.

5. Conclusions

[58] Coupled climate carbon model simulations provide an important tool for characterizing potential climate responses in future ocean ecology and biogeochemistry [e.g., *Steinacher et al*., 2010]. Based on the CCSM-3 model simulations, we project large-scale shifts of phytoplankton surface community structure, biomass, and productivity in response to anthropogenic climate change over the last several decades of the 20th century and the 21st century.

[59] In CCSM-3, climate warming drives small global decreases in phytoplankton biomass and productivity by decreasing the nutrient supply to the surface, particularly in the equatorial, LLU, and subtropics which dominate (in terms of area and present phytoplankton biomass) the global budgets. As such, we suggest that future modeling studies explicitly save nutrient budget terms to allow a more precise quantification of the climate driven changes in nutrient supply terms—advective versus diffusive, horizontal versus vertical—than we were able to perform here.

[60] The competition between (a) the stratifying effects of warmer temperatures and freshening and (b) the destratifying effects of increasing wind strength—controls nutrient supply to the euphotic layer and, to a large degree, phytoplankton dynamics. Over the 21st century, differential increases in temperature, stratification, and midlatitude westerlies in the two hemispheres are responsible for the different ecological responses of the Southern and Northern Hemisphere. A stronger decrease in surface salinity and more surface warming result in more stabilization of the water column and a more significant decrease in nutrient supply to the surface in the NH compared to the SH (Figures 4c and 4e). The resulting decrease in surface nitrogen primarily explains the decreases in diatom and small phytoplankton biomass in the Northern equatorial, low-latitude upwelling, subtropical, and subpolar biomes and drives the average decreases in NH phytoplankton chlorophyll, biomass, primary, and export production with global warming (Figures 4h, 4i, 4j).

[61] Increased temperatures and enhanced midlatitude westerlies govern the ecological response to climate change in the SH subtropical and subpolar biomes. A stronger increase in westerlies contributes to a smaller climate-driven increase in stratification in the SH compared to the NH, and ultimately smaller nutrient declines in the SH compared to the equivalent NH biomes over the 21st century. Temperature increases directly contribute to diatom growth increases in the SH subtropical and subpolar biomes, compensating for some of the nutrient-driven biomass declines in these biomes. Poleward shifts and intensification in high-latitude westerlies result in increased vertical upwelling of Fe south of 50°S, southward shifts in the Southern Ocean subtropical-subpolar boundary and the corresponding diatom biomass maximum, and an intensified Ekman transport convergence of heat and diatom biomass at the southward migrating subtropical-subpolar boundary. These factors contribute to significant increases in the SH subpolar diatom biomass and primary production over the 21st century (Figures 2b and 7c). The observed increase in diatoms with increasing Southern westerlies over the 21st century nicely parallels the hypothesized phytoplankton behavior at the last deglaciation. During the last deglaciation, increased westerlies likely resulted in increased upwelling of nutrient rich waters south of the Antarctic Polar Front, and enhanced diatom growth, as evidenced by a higher silicate flux reaching the bottom ocean sediments [*Anderson et al*., 2009].

[62] Grazing is the dominant loss for phytoplankton in both the real ocean [*Banse*, 1994] and in our model. Modelers are aware of the profound influence that the equations and parameter choice for representing zooplankton and phytoplankton-zooplankton interactions have on simulated plankton stocks and primary production [e.g., *Franks et al*., 1986; *Fasham*, 1995], export fluxes [*Anderson et al*., 2010], food web dynamics and structure [e.g., *Gentleman and Neuheimer*, 2008; *Sailley et al*., 2013, *Hashioka et al*., 2013] or phytoplankton diversity [*Prowe et al*., 2012]. The current generation of complex Earth System Models uses widely different parameterizations for grazing and therefore show wide differences in the relative contributions of bottom up versus top-down factors in the control of phytoplankton blooms [*Hashioka et al*., 2013]. Our model includes only one generic zooplankton dependent on prey biomass via a Holling type III function. *Sailley et al*. [2013] recently showed that the effect of the generic zooplankton grazing on phytoplankton functional types (PFTs) in the CCSM-BEC is similar to a density-dependent mortality term; the PFTs cannot escape grazing by the generic zooplankton such that blooms and PFT variability are stifled by a strong top-down control. Since specific grazing rate of the generic zooplankton on small phytoplankton is larger than on diatoms, top-down control leads to an increase in the percent of diatoms in all blooms. In our model, dominance of diatoms is thus mainly determined by top-down control while dominance of small phytoplankton is determined by bottom-up (primarily nutrient) control, as recently shown by *Hashioka et al*. [2013]. Given our current knowledge and the complexity of the system, it is unclear apriori how the PFT responses to climate change found in this paper would evolve if more sophisticated grazing formulations (e.g., a size-structured zooplankton population) were included.

[63] One caveat in our work is that our coarse resolution model cannot explicitly resolve eddy dynamics. An enhanced eddy-induced circulation under a more positive Southern Annular Mode acts to flatten the Southern Ocean isopycnals, counterbalancing some of the changes in the Ekman-induced mean circulation. The extent to which eddies can compensate the mean-flow and the repercussions on carbon cycling are topics of active research in both modeling and observational communities at this point in time [e.g., *Hallberg and Gnanadesikan*, 2006; *Böning et al*., 2008; *Farneti and Delworth*, 2010; *Ito et al*., 2010; *Meredith et al*., 2012; *Sallee et al*., 2012]. It is possible that future higher-resolution or

eddy-resolving climate models, in which eddy dynamics is resolved rather than parameterized, will result in smaller wind-driven changes in Southern Ocean dynamics than our current Intergovernmental Panel on Climate Change Fifth Assessment Report (IPCC AR5) class coupled models suggest, implying less Northern Hemisphere–Southern Hemisphere asymmetry in the biogeochemical and ecological response to future climate change.

[64] Further research needs to clarify the long-term fate of midlatitude westerlies, the underlying physical mechanism for many ocean features noted in this paper. Changes in midlatitude westerlies depend on a competition between the rate of greenhouse gas emissions and the rate at which the ozone hole closes. Uncertainties in the aerosol and cloud responses aside, the question becomes whether the acceleration of greenhouse gas emissions (which acts to intensify the westerlies) will overcome the rate at which the ozone hole closes, and whether the winds will continue to shift, or even reverse direction, after the closing of the ozone hole [e.g, *Polvani et al*., 2011; *Simpkins and Karpechko*, 2012]. Since the main physical changes in winds and ocean circulation observed in the National Center for Atmospheric Research Community Climate System Model, version 3.0 (NCAR CCSM-3) should broadly hold across the latest generation of global climate-carbon models, we find it likely that the ecological and biogeochemical interhemispheric contrasts discussed here will also hold across the IPCC AR5 models (A. Cabre et al., Consistent global responses of marine ecosystems to future climate change across the IPCC AR5 earth system models, manuscript in preparation, 2013).

Appendix A

[65] In the CCSM-3 model the diatom, small phytoplankton, and diazotroph chlorophyll and biomass (carbon) tracers each are determined by an equation of the form:

$$\frac{\partial P_x}{\partial t} + \nabla\cdot\left(\vec{u}P_x\right) - \nabla\cdot(K\cdot\nabla P_x) = \mu_x\cdot P - G(P_x) - m_x\cdot P_x - A(P_x) \tag{A1}$$

where the left-hand side terms include advection and diffusion, and the biological terms on the right-hand side represent a source term due to growth and multiple sinks due to grazing, linear mortality, and aggregation of particles ($A(P_x)$, square dependence on P_x). The largest loss term is due to grazing, which is parameterized as a Holling type III functional response and is higher for small phytoplankton than for diatoms. The photosynthetic specific growth rate μ_x for each phytoplankton type x (diatoms, small phytoplankton, and diazotrophs) is the product of a temperature function (T_f), a nutrient limitation term (V_x) and a light availability function (L_x):

$$\mu_x = \mu_x^{ref}\cdot T_f\cdot V_x\cdot L_x \tag{A2}$$

where maximum phytoplankton C-specific growth rate μ_x^{ref} is 3 day^{-1} for diatoms and small phytoplankton and 0.4 day^{-1} for diazotrophs [*Moore et al*., 2002]. The temperature function T_f is a Q10 function of temperature and is identical for all phytoplankton, while the individual phytoplankton types have different nutrient and light requirements, i.e., different V_x and L_x.. The light function L_x follows a modified form of the *Geider et al*. [1998] dynamic growth model and includes photo-adaptation parameterized with adaptive Chl/C ratios.

[66] For each of the three phytoplankton types, the most limiting nutrient governs the nutrient limitation term:

$$V_{diat} = min\left(V_{diat}^{Fe}, V_{diat}^{N}, V_{diat}^{SiO_3}, V_{diat}^{PO_4}\right);$$
$$V_{sp} = min\left(V_{sp}^{Fe}, V_{sp}^{N}, V_{sp}^{PO_4}\right); V_{diaz} = min\left(V_{diaz}^{Fe}, V_{diaz}^{PO_4}\right) \tag{A3}$$

$$where V_x^{NO_3} = \frac{\frac{NO_3}{K_x^{NO_3}}}{1 + \frac{NO_3}{K_x^{NO_3}} + \frac{NH_4}{K_x^{NH_4}}};$$

$$V_x^{NH_4} = \frac{\frac{NH_4}{K_x^{NH_4}}}{1 + \frac{NO_3}{K_x^{NO_3}} + \frac{NH_4}{K_x^{NH_4}}}; V_x^{N} = V_x^{NO_3} + V_x^{NH_4}$$

$$V_x^{PO_4} = \frac{PO_4}{PO_4 + K_x^{PO_4}}; V_x^{Fe} = \frac{Fe}{Fe + K_x^{Fe}}; V_x^{SiO_3} = \frac{SiO_3}{SiO_3 + K_x^{SiO_3}} \tag{A4}$$

Climate change modifies the growth rate of phytoplankton via changes in light, nutrients, and temperature. In *Marinov et al*. [2010], we separated analytically these effects by calculating:

$$\Delta\mu_x = \Delta\mu_x^{light} + \Delta\mu_x^{nutr} + \Delta\mu_x^{temp} \tag{A5}$$

[67] Where

$$\Delta\mu_x^{light} = \alpha_x\theta_x^c I_{par}\cdot\left(\frac{\Delta I_{par}}{I_{par}} - \frac{\Delta V_x}{V_x} - \frac{\Delta T_f}{T_f}\right)\cdot\exp\left(\frac{-\alpha_x\cdot\theta_x^c\cdot I_{par}}{\mu_{ref} V_x T_f}\right) \tag{A6a}$$

$$\Delta\mu_x^{nutr} = \mu_{ref}\cdot T_f L_x\cdot\Delta V_x \tag{A6b}$$

$$\Delta\mu_x^{temp} = \mu_{ref}\cdot L_x V_x\cdot\Delta T_f \tag{A6c}$$

where α_x (mmolC m^2 (mgChl W d)$^{-1}$) is the initial slope of the photosynthesis-irradiance (P-I) curve for phytoplankton type x assumed to be 0.3 for diatoms and small phytoplankton, 0.036 for diazotrophs; θ_x^c is the Chl/C ratio, I_{par} is irradiance. I_{par}, V_x, and T_f represent the initial state taken for us to be the average for years 1980–1999, and the Δ notation refers to small perturbations around this state, calculated in this paper as the difference between years 1980–1999 and 2080–2099. Climate driven changes in diatom and small phytoplankton growth rates due to light, nutrient, and temperature (calculated from equations (A6a), (A6b), (A6c)) are shown in Figure 8 for the various biomes. Zonal averages for these terms for the global ocean are shown in Figure S1.

Appendix B

[68] We define a set of ecological biomes based on physical criteria, closely following the definitions employed by

Sarmiento et al. [2004] and conceptually along the lines of *Longhurst* [1994]. We use the sign of the annual mean vertical velocity at 50 m (layer 5 in the model), the extent of the ice coverage, and the maximum mixed layer depth based on monthly analyses to determine our principal biogeographical provinces or "ecological biomes", illustrated in Figure 6.

[69] The equatorial domain is the 5°S to 5°N region, which can be divided further into upwelling and downwelling subregions. The low-latitude upwelling biome (LLU) contains upwelling regions between 5°S–35°S and 5°N–30°N. This is primarily a high-nutrient supply and high-productivity region along the continental western margins. The subpolar biome is the region north of 30°N and south of 35°S (outside of the LLU and ice biomes) where there is upwelling. The marginal sea ice biome is the geographical province covered by sea ice during some part of the year.

[70] Finally, the subtropical region is the region outside the equatorial domain defined by downwelling at 50 m. The subtropical region can be further divided into a permanently stratified subtropical biome, where the maximum mixed layer depth (based on monthly analyses) does not exceed 150 m, and a seasonally stratified subtropical biome, where the maximum mixed layer depth exceeds 150 m. Winter convection in the seasonally stratified region injects nutrients into the euphotic zone, allowing for seasonal blooms, and therefore higher biomass and productivity. When calculating average ecological properties over all biomes, we exclude marginal bodies of water (Mediterranean Sea, Baltic Sea, Red Sea, Persian Gulf, and Hudson Bay) but, unlike *Sarmiento et al*. [2004], we take into account the entire Arctic Ocean. We divide the Atlantic from the Indian at 19°E, the Indian from the Pacific at 150°E, and the Pacific from the Atlantic Ocean at 71°W.

[71] **Acknowledgments.** I. Marinov was supported by National Science Foundation (NSF) Grant ATM06-28582 while at WHOI and by NASA Grant NNX13AC92G while at Penn. I. Lima and S. Doney were supported by the Center for Microbial Oceanography, Research, and Education (CMORE), an NSF Science and Technology Center (EF-0424599). The CCSM-3 simulations were integrated with computer resources from the NCAR Climate Simulation Laboratory. The National Center for Atmospheric Research is sponsored by the National Science Foundation. We are indebted to the numerous scientists and programmers who have contributed to the Community Climate System Model, and in particular we thank the members of the CCSM Biogeochemistry Working Group. I.M. thanks A. Cabre and S. Leung for numerous discussions on modeling ocean ecology; R. Bernardello and J. Palter for discussions on nutrient fluxes.

References

Anderson, R. F., S. Ali, L. I. Bradtmiller, S. H. H. Nielsen, M. Q. Fleisher, B. E. Anderson, and L. H. Burckle (2009), Wind-driven upwelling in the Southern Ocean and the deglacial rise in atmospheric CO_2, *Science*, *323*(5920), 1443–1448, doi:10.1126/science.1167441.

Anderson, T. R., W. C. Gentleman, and B. Sinha (2010), Influence of grazing formulations on the emergent properties of a complex ecosystem model in a global ocean general circulation model, *Prog. Oceanogr.*, *87*(1–4), 201–213.

Antoine, D., A. Morel, H. R. Gordon, V. F. Banzon, and R. H. Evans (2005), Bridging ocean color observations of the 1980s and 2000s in search of long-term trends, *J. Geophys. Res.*, *110*, C06009, doi:10.1029/2004JC002620.

Banse, K. (1994), Grazing and zooplankton production as key controls of phytoplankton production in the open ocean, *Oceanography*, *7*, 13–20.

Barnes, E. A., and L. M. Polvani (2013), Response of the midlatitude jets and of their variability to increased greenhouse gases in the CMIP5 models, *J. Climate*, *26*, 7117–7135, doi:10.1175/JCLI-D-12-00536.1.

Behrenfeld, M. J., R. T. O'Malley, D. A. Siegel, C. R. McClain, J. L. Sarmiento, G. C. Feldman, A. J. Milligan, P. G. Falkowski, R. M. Letelier, and E. S. Boss (2006), Climate-driven trends in contemporary ocean productivity, *Nature*, *444*, 752–755, doi:10.1038/nature05317.

Böning, C. W., A. Dispert, M. Visbeck, S. R. Rintoul, and F. U. Schwarzkopf (2008), The response of the Antarctic Circumpolar Current to recent climate change, *Nat. Geosci.*, *1*, 864–869, doi:10.1038/ngeo362.

Bopp, L., P. Monfray, O. Aumont, J. L. Dufresne, H. Le Treut, G. Madec, L. Terray, and J. C. Orr (2001), Potential impact of climate change on marine export production, *Global Biogeochem. Cycles*, *15*, 81–99.

Bopp, L., O. Aumont, P. Cadule, S. Alvain, and M. Gehlen (2005), Response of diatoms distribution to global warming and potential implications: A global modeling study, *Geophys. Res. Letters*, *32*, L19606, doi:10.1029/2005GL023653.

Bopp, L., et al. (2013), Multiple stressors of ocean ecosystems in the 21st century: Projections with CMIP5 models, *Biogeosciences*, *10*, 3627–3676, doi:10.5194/bgd-10-3627-2013.

Bryan, K., S. Manabe, and M. J. Spelman (1988), Interhemispheric asymmetry in the transient response of a coupled ocean-atmosphere model to a CO2 forcing, *J. Phys. Oceanogr.*, *18*(6), 851–867, doi:10.1175/1520-0485(1988).

Cai, W., T. Cowan, S. Godfrey, and S. Wijffels (2010), Simulations of processes associated with the fast warming rate of the Southern Midlatitude Ocean, *J. Climate*, *23*, 197–206, doi:10.1175/2009JCLI3081.1.

Capotondi, A., M. A. Alexander, N. A. Bond, E. N. Curchitser, and J. D. Scott (2012), Enhanced upper ocean stratification with climate change in the CMIP3 models, *J. Geophys. Res.*, *117*, C04031, doi:10.1029/2011JC007409.

Cermeno, P., S. Dutkiewicz, R. P. Harris, M. Follows, O. Schofield, and P. G. Falkowski (2008), The role of nutricline depth in regulating the ocean carbon cycle, *Proc. Natl. Acad. Sci. U. S. A.*, *105*, doi:10.1073/pnas.0811302106.

Collins, W. D., et al. (2006), The Community Climate System Model Version 3 (CCSM3), *J. Climate*, *19*(11), 2122–2143, doi:10.1175/JCLI3761.1.

Doney, S. C. (2006), Plankton in a warmer world, *Nature*, *444*, 695–696.

Doney, S. C., K. Lindsay, I. Fung, and J. John (2006), Natural variability in a stable 1000 year coupled climate-carbon cycle simulation, *J. Climate*, *19*(13), 3033–3054.

Doney, S. C., I. Lima, J. K. Moore, K. Lindsay, M. J. Behrenfeld, T. K. Westberry, N. Mahowald, D. M. Glover, and T. Takahashi (2009a), Skill metrics for confronting global upper ocean ecosystem-biogeochemistry models against field and remote sensing data, *J. Mar. Syst.*, *76*, 95–112, doi:10.1016/j.jmarsys.2008.05.015.

Doney, S. C., I. Lima, R. A. Feely, D. M. Glover, K. Lindsay, N. Mahowald, J. K. Moore, and R. Wanninkhof (2009b), Mechanisms governing interannual variability in upper-ocean inorganic carbon system and air-sea CO_2 fluxes: Physical climate and atmospheric dust, *Deep Sea Res. Part II*, *56*, 640–655.

Dufresne, J. L., J. Quaas, O. Boucher, S. Denvil, and L. Fairhead (2005), Contrasts in the effects on climate of anthropogenic sulfate aerosols between the 20th and the 21st century, *Geophys. Res. Lett.*, *32*, L21703, doi:10.1029/2005GL023619.

Falkowski, P. G., R. T. Barber, and V. Smetacek (1998), Biogeochemical controls and feedbacks on ocean primary production, *Science*, *281*(5374), 200–206.

Farneti, R., and T. L. Delworth (2010), The role of mesoscale eddies in the remote oceanic response to altered Southern Hemisphere winds, *J. Phys. Oceanogr.*, *40*(10), 2348–2354, doi:10.1175/2010JPO4480.1.

Fasham, M. J. R. (1995), Variations in the seasonal cycle of biological production in subarctic oceans—A model sensitivity analysis, *Deep Sea Res. Part I*, *42*, 1111–1149.

Flato, G. M., and G. J. Boer (2001), Warming asymmetry in climate change simulations, *Geophys. Res. Lett.*, *28*(1), 195, doi:10.1029/2000GL012121.

Franks, P. J. S., J. S. Wroblewski, and G. R. Flierl (1986), Behavior of a simple plankton model with food-level acclimation by herbivores, *Mar. Biol.*, *91*, 121–129.

Geider, R. J., H. L. MacIntyre, and T. M. Kana (1998), A dynamic regulatory model of phytoplankton acclimation to light, nutrients, and temperature, *Limnol. Oceanogr.*, *43*, 679–694.

Gent, P. R., and G. Danabasoglu (2011), Response of increasing Southern Hemisphere winds in CCSM3.1, *J. Climate*, *24*(19), 4992–4998, doi:10.1175/JCLI-D-10-05011.1.

Gentleman, W. C., and A. B. Neuheimer (2008), Functional responses and ecosystem dynamics: How clearance rates explain the influence of satiation, food-limitation and acclimation, *J. Plankton Res.*, *30*, 1215–1231.

Gnanadesikan, A., J. P. Dunne, and J. John (2011), What ocean biogeochemical models can tell us about bottom-up control of ecosystem variability, *ICES J. Mar. Sci.*, *68*(6), 1030–1044, doi:10.1093/icesjms/fsr098.

Gregg, W. W., M. E. Conkright, P. Ginoux, J. E. O'Reilly, and N. W. Casey (2003), Ocean primary production and climate: Global decadal changes, *Geophys. Res. Lett.*, *30*(15), 1809, doi:10.1029/2003GL016889.

Gregg, W. W., N. W. Casey, and C. R. McClain (2005), Recent trends in global ocean chlorophyll, *Geophys. Res. Lett.*, *32*, L03606, doi:10.1029/2004GL021808.

Hallberg, R., and A. Gnanadesikan (2006), The role of eddies in determining the structure and response of the wind-driven southern hemisphere overturning: Results from the Modeling Eddies in the Southern Ocean (MESO) project, *J. Phys. Oceanogr.*, *36*(12), 2232–2252, doi:10.1175/JPO2980.1.

Hashioka, T., et al. (2013), Phytoplankton competition during the spring bloom in four plankton functional type models, *Biogeosciences*, *10*, 6833–6850, doi:10.5194/bg-10-6833-2013.

Henson, S. A., J. L. Sarmiento, J. P. Dunne, L. Bopp, I. Lima, S. C. Doney, J. John, and C. Beaulieu (2010), Detection of anthropogenic climate change in satellite records of ocean chlorophyll and productivity, *Biogeosciences*, *7*(2), 621–640.

Hutchinson, D. K., M. H. England, A. Santoso, and A. M. Hogg (2013), Interhemispheric asymmetry in transient global warming: The role of Drake Passage, *Geophys. Res. Lett.*, *40*, 1587–1593, doi:10.1002/grl.50341.

Ito, T., M. Woloszyn, and M. Mazloff (2010), Anthropogenic carbon dioxide transport in the Southern Ocean driven by Ekman flow, *Nature*, *463*, 80–83, doi:10.1038/nature08687.

Le Quere, C., et al. (2007), Saturation of the Southern Ocean CO_2 sink due to recent climate change, *Science*, *316*(5832), 1735–1738, doi:10.1126/science.1136188.

Longhurst, A. (1994), *Ecological Geography of the Ocean*, pp. 176, Academic, San Diego, Calif.

Lovenduski, N. S., N. Gruber, S. C. Doney, and I. D. Lima (2007), Enhanced CO_2 outgassing in the Southern Ocean from a positive phase of the Southern Annular Mode, *Global Biogeochem. Cycles*, *21*, GB2026, doi:10.1029/2006GB002900.

Lovenduski, N. S., N. Gruber, and S. C. Doney (2008), Toward a mechanistic understanding of the decadal trends in the Southern Ocean carbon sink, *Global Biogeochem. Cycles*, *22*, GB3016, doi:10.1029/2007GB003139.

Mahowald, N. M., et al. (2010), Observed 20th century desert dust variability: Impact on climate and biogeochemistry, *Atmos. Chem. Phys.*, *10*(22), 10,875–10,893, doi:10.5194/acp-10-10875-2010.

Manabe, S., R. J. Stouffer, M. J. Spelman, and K. Bryan (1991), Transient responses of a coupled ocean-atmosphere model to gradual changes of atmospheric CO_2. Part I. Annual mean response, *J. Climate*, *4*(8), 785–818, doi:10.1175/1520-0442(1991)004<0785:TROACO>2.0.CO;2.

Marinov, I., A. Gnanadesikan, J. L. Sarmiento, J. R. Toggweiler, M. Follows, and B. K. Mignone (2008), Impact of oceanic circulation on biological carbon storage in the ocean and atmospheric pCO_2, *Global Biogeochem. Cycles*, *22*, GB3007, doi:10.1029/2007GB002958.

Marinov, I., S. C. Doney, and I. D. Lima (2010), Response of ocean phytoplankton community structure to climate change over the 21st century: partitioning the effects of nutrients, temperature and light, *Biogeosciences*, *7*, 3941–3959, doi:10.5194/bg-7-3941-2010.

Martinez, E., D. Antoine, F. D'Ortenzio, and B. Gentili (2009), Climate-driven basin-scale decadal oscillations of oceanic phytoplankton, *Science*, *326*(5957), 1253–1256, doi:10.1126/science.1177012.

McGillicuddy, D. J. Jr., L. A. Anderson, S. C. Doney, and M. E. Maltrud (2003), Eddy-driven sources and sinks of nutrients in the upper ocean: Results from a 0.1° resolution model of the North Atlantic, *Global Biogeochem. Cycles*, *17*, 1035, doi:10.1029/2002GB001987,2.

Meehl, G., et al. (2007), Global Climate Projections, in *Climate Change 2007: The Physical Science Basis. Contribution of Working Group I to the Fourth Assessment Report of the Intergovernmental Panel on Climate Change*, edited by S. Solomon et al., pp. 747–845, Cambridge Univ. Press, Cambridge, U.K.

Meredith, M. P., A. C. Naveira Garabato, A. M. Hogg, and R. Farneti (2012), Sensitivity of the overturning circulation in the Southern Ocean to decadal changes in wind forcing, *J. Climate*, *25*(1), 99–110, doi:10.1175/2011JCLI4204.1.

Moore, J. K., S. C. Doney, J. C. Kleypas, D. M. Glover, and I. Y. Fung (2002), An intermediate complexity marine ecosystem model for the global domain, *Deep Sea Res. Part II*, *49*, 403–462.

Moore, J. K., S. C. Doney, and K. Lindsay (2004), Upper ocean ecosystem dynamics and iron cycling in a global three-dimensional model, *Global Biogeochem. Cycles*, *18*, GB4028, doi:10.1029/2004GB002220.

Moore, J. K., S. C. Doney, K. Lindsay, N. Mahowald, and A. F. Michaels (2006), Nitrogen fixation amplifies the ocean biogeochemical response to decadal timescale variations in mineral dust deposition, *Tellus B Chem. Phys. Meteorol.*, *58*(5), 560–572.

Polvani, L. M., M. Previdi, and C. Deser (2011), Large cancellation, due to ozone recovery, of future Southern Hemisphere atmospheric circulation trends, *Geophys. Res. Lett.*, *38*, L04707, doi:10.1029/2011GL046712.

Prowe, F., M. Pahlow, S. Dutkiewicz, M. Follows, and A. Oschlies (2012), Top-down control of marine phytoplankton diversity in a global ecosystem model, *Prog. Oceanogr.*, *101*, 1–13, doi:10.1016/j.pocean.2011.11.016.

Russell, J., K. Dixon, A. Gnanadesikan, R. Stouffer, and J. R. Toggweiler (2006), The Southern Hemisphere Westerlies in a Warming World: Propping open the door to the deep ocean, *J. Climate*, *19*(24), 6382–6390.

Sailley, S., M. Vogt, S. C. Doney, M. N. Aita, L. Bopp, E. T. Buintenhuis, T. Hashioka, I. Lima, C. Le Quéré, and Y. Yamanaka (2013), Comparing food web structures and dynamics across a suite of global marine ecosystem models, *Ecol. Model.*, *261*, 43–57, doi:10.1016/j.ecolmodel.2013.04.006.

Sallee, J. B., R. J. Matear, S. R. Rintoul, and A. Lenton (2012), Localized subduction of anthropogenic carbon dioxide in the Southern Hemisphere Oceans, *Nat. Geosci.*, *5*(8), 579–584, doi:10.1038/NGEO1523.

Sarmiento, J. L., et al. (2004), Response of ocean ecosystems to climate warming, *Global Biogeochem. Cycles*, *18*, GB3003, doi:10.1029/2003GB002134.

Schmittner, A., A. Oschlies, H. D. Matthews, and E. D. Galbraith (2008), Future changes in climate, ocean circulation, ecosystems, and biogeochemical cycling simulated for a business-as-usual CO_2 emission scenario until year 4000 AD, *Global Biogeochem. Cycles*, *22*, GB1013, doi:10.1029/2007GB002953.

Sen Gupta, A., A. Santoso, A. S. Taschetto, C. C. Ummenhofer, J. Trevena, and M. H. England (2009), Projected changes to the Southern Hemisphere Ocean and sea ice in the IPCC AR4 climate models, *J. Climate*, *22*, 3047–3078, doi:10.1175/2008JCLI2827.1.

Siegel, D. A., et al. (2013), Regional to global assessments of phytoplankton dynamics from the SeaWiFS mission, *Remote Sens. Environ.*, *135*, 77–91, doi:10.1016/j.rse.2013.03.025.

Simpkins, G. R., and A. Y. Karpechko (2012), Sensitivity of the southern annular mode to greenhouse gas emission scenarios, *Clim. Dyn.*, *38*(3–4), 563–572, doi:10.1007/s00382-011-1121-2.

Smith, R. D., and P. R. Gent (2002), Reference manual for the Parallel ocean Program (POP), ocean component of the Community Climate System Model (CCSM2.0 and 3.0). Tech. Rep. LA-UR-02-2484, *Los Alamos National Laboratory* [Available online at http://www.ccsm.ucar.edu/models/ccsm3.0/pop.].

Solomon, S., D. Qin, M. Manning, Z. Chen, M. Marquis, K. B. Averyt, M. Tignor, and H. L. Miller (Eds) (2007), *Contribution of Working Group I to the Fourth Assessment Report of the Intergovernmental Panel on Climate Change*, Cambridge Univ. Press, Cambridge, U. K., and New York.

Steinacher, M., et al. (2010), Projected 21st century decrease in marine productivity: a multi-model analysis, *Biogeosciences*, *7*, 979–1005.

Straile, D. (1997), Gross growth efficiencies of protozoan and metazoan zooplankton and their dependence on food concentration, predator-prey weight ratio, and taxonomic group, *Limnol. Oceanogr.*, *42*, 1375–1385.

Swart, N. C., and J. C. Fyfe (2012), Observed and simulated changes in the Southern Hemisphere surface westerly wind-stress, *Geophys. Res. Lett.*, *39*, L16711, doi:10.1029/2012GL052810.

Taucher, J., and A. Oschlies (2011), Can we predict the direction of marine primary production change under global warming?, *Geophys. Res. Lett.*, *38*, L02603, doi:10.1029/2010GL045934.

Thompson, D. W. J., and S. Solomon (2002), Interpretation of recent Southern Hemisphere climate change, *Science*, *296*, 895–899.

Thornton, P. E., S. C. Doney, K. Lindsay, J. K. Moore, N. M. Mahowald, J. T. Randerson, I. Y. Fung, J. F. Lamarque, J. J. Feddema, and Y.-H. Lee (2009), Carbon-nitrogen interactions regulate climate-carbon cycle feedbacks: Results from an atmosphere-ocean general circulation model, *Biogeoscience*, *6*(10), 2099–2120.

Toggweiler, J. R., J. L. Russell, and S. R. Carson (2006), Midlatitude westerlies, atmospheric CO_2, and climate change during the ice ages, *Paleoceanography*, *21*, PA2005, doi:10.1029/2005PA001154.

Wang, M., and J. E. Overland (2009), A sea ice free summer Arctic within 30 years?, *Geophys. Res. Lett.*, *36*, L07502, doi:10.1029/2009GL037820.

Williams, R. G., and M. J. Follows (1998), The Ekman transfer of nutrients and maintenance of new production over the North Atlantic, *Deep Sea Res. Part I*, *45*(2–3), 461–489, doi:10.1016/S0967-0637(97)00094-0.

Williams, R. G., A. J. McLaren, and M. J. Follows (2000), Estimating the convective supply of nitrate and implied variability in export production over the North Atlantic, *Global Biogeochem. Cycles*, *14*(4), 1299–1313, doi:10.1029/2000GB001260.

Yeager, S. G., C. A. Shields, W. G. Large, and J. J. Hack (2006), The low-resolution CCSM3, *J. Climate*, *19*, 2545–2566.

Yin, J. H. (2005), A consistent poleward shift of the storm tracks in simulations of 21st century climate, *Geophys. Res. Lett.*, *32*, L18701, doi:10.1029/2005GL023684.

Yoder, J. A., M. A. Kennelly, S. C. Doney, and I. D. Lima (2010), Are trends in SeaWiFS chlorophyll time-series unusual relative to historic variability?, *Acta Oceanolog. Sin.*, *29*(2), 1–4.